ResearchGate

See discussions, stats, and author profiles for this publication at: https://www.researchgate.net/publication/333437331

Hydrothermal eruptions at unstable crater lakes: Insights from the Boiling Lake, Dominica, Lesser Antilles

Article *in* Journal of Volcanology and Geothermal Research · May 2019

DOI: 10.1016/j.jvolgeores.2019.05.020

CITATIONS
5

READS
1,074

6 authors, including:

Stefanie Rott
Ludwig-Maximilians-University of Munich
6 PUBLICATIONS **85** CITATIONS
SEE PROFILE

Betty Scheu
Ludwig-Maximilians-Universität München (LMU)
209 PUBLICATIONS **3,367** CITATIONS
SEE PROFILE

Cristian Montanaro
Ludwig-Maximilians-University of Munich
35 PUBLICATIONS **495** CITATIONS
SEE PROFILE

Erouscilla P Joseph
University of the West Indies, St. Augustine
31 PUBLICATIONS **312** CITATIONS
SEE PROFILE

Some of the authors of this publication are also working on these related projects:

Project
Experimental Chaotic Mixing View project

Project
Quantification and Characterization of Strain During Flow-Induced Deformation of Tuffs and Lavas View project

All content following this page was uploaded by Stefanie Rott on 24 June 2019.

The user has requested enhancement of the downloaded file.

Journal of Volcanology and Geothermal Research 381 (2019) 101–118

Contents lists available at ScienceDirect

Journal of Volcanology and Geothermal Research

journal homepage: www.elsevier.com/locate/jvolgeores

Hydrothermal eruptions at unstable crater lakes: Insights from the Boiling Lake, Dominica, Lesser Antilles

Stefanie Rott [a,*], Bettina Scheu [a], Cristian Montanaro [a,b], Klaus Mayer [a], Erouscilla P. Joseph [c], Donald B. Dingwell [a]

[a] Department of Earth and Environmental Sciences, Ludwig-Maximilians-Universität München (LMU), Theresienstrasse 41/III, 80333 Munich, Germany
[b] School of Environment – University of Auckland, New Zealand
[c] Seismic Research Centre, University of the West Indies, St. Augustine, Trinidad and Tobago

ARTICLE INFO

Article history:
Received 18 December 2018
Received in revised form 16 May 2019
Accepted 23 May 2019
Available online 28 May 2019

Keywords:
Hydrothermal eruptions
Alteration
Volcanic lakes
Decompression experiments
Hazard assessment

ABSTRACT

The Boiling Lake - a major touristic attraction in the Morne Trois Pitons National Park, Dominica's (West Indies) World Heritage site - is located in an area of high hydrothermal activity in the southern part of the island. This spectacular lake is characterized by unstable behavior which has been interpreted to result from the presence of a water body above a fluctuating gas-filled, or multi-phase vent system. The system produces a near-boiling lake that occasionally drains and refills with water, without any simple periodicity. Despite the fact that such unstable draining lakes are thought to be non-eruptive, the Boiling Lake is known to have sourced occasional small hydrothermal eruptions as well as toxic gas emissions which accompany the refilling phase of these drainage events. Similar explosive events seem also to be likely after landslide slumped rocks from steep altered crater walls cover the vent area in the lake leading to overpressurized conditions. In both cases, rock expulsion and gas release continue to pose serious threats for tourists and tour guides. While conceptual models exist describing possible mechanisms of the Boiling Lake drainage itself, little information exists to date regarding the trigger mechanisms related to the explosive events. Further, no estimation of the eruption processes and dynamics of these events has previously been attempted. To address this knowledge gap, we employ here a combined field- and laboratory-based approach in order to i) characterize the properties of the dominant lithologies from the crater walls at Boiling Lake, ii) determine how the ongoing alteration may affect their petrophysical properties (e.g., porosity and permeability), and iii) evaluate how water-saturated, unconsolidated wall rock materials behave when rapidly decompressed from a slightly elevated pressure and temperature conditions.

Here, we propose that it is the petrophysical state of the materials involved (e.g. porosity, permeability and alteration-related strength) which controls the style and energy of these eruptions, as well as the potential for landslides from the crater walls. The experimentally simulated scenarios included in this study are: i) decompression from only slightly elevated pressure conditions inferred for small hydrothermal eruptions occurring after lake drainage events, and ii) decompression from rapidly enhanced pressure conditions produced by the capping and overpressurization of the vent area following landslide episodes. Ejection velocities obtained from rapid decompression experiments were used as input parameters for ballistic trajectory calculations, allowing for estimation of the potential area impacted by ejected debris.

We anticipate that this study will serve as a contribution to the understanding of the hazard potential of future hydrothermal eruptions at unstable crater lakes in general, as well as providing direct insights into the ongoing hydrothermal activity at the Boiling Lake.

© 2019 The Authors. Published by Elsevier B.V. This is an open access article under the CC BY-NC-ND license (http://creativecommons.org/licenses/by-nc-nd/4.0/).

1. Introduction

The Boiling Lake is one of Dominica's most popular tourist attractions: the world's second largest high-temperature crater lake (Di Napoli et al., 2013). Its spectacular nature is due to an unstable and delicate physical state produced by a denser liquid layer (a lake) placed atop a gas- or multi-phase-filled vent system. The instability is manifested as a near-boiling lake that occasionally drains and refills its water, without a clear periodicity (Fournier et al., 2009). Together with the nearby Valley of Desolation, they represent the most active hydrothermal areas in the Morne Trois Pitons National Park of Dominica (Joseph et al., 2011), drawing ~80,000 tourists per year (James, pers. comm.). Many of the crater-like features in these areas, Boiling Lake

* Corresponding author.
E-mail address: stefanie.rott@min.uni-muenchen.de (S. Rott).

https://doi.org/10.1016/j.jvolgeores.2019.05.020
0377-0273/© 2019 The Authors. Published by Elsevier B.V. This is an open access article under the CC BY-NC-ND license (http://creativecommons.org/licenses/by-nc-nd/4.0/).

included, have been formed as a result of steam-driven phreatic/hydrothermal eruptions, and/or following magmatic intrusions resulting in phreatomagmatic explosive events (Lindsay et al., 2005a, 2005b; Fournier et al., 2009; Mayer et al., 2017). Some of the best-known unstable draining lakes are generally non-eruptive, for example the lake filling the Inferno Crater in New Zealand, whose level changes by nearly 10 m with a typical period of about 30 to 50 days following variations in the geothermal activity, or seismic events (Vandemeulebrouck et al., 2005; Vandemeulebrouck et al., 2008). Boiling Lake, in contrast, is known to have produced occasional small, and deadly toxic gas emissions and/or hydrothermal eruptions associated with the crater refilling phases (Fournier et al., 2009; Lindsay et al., 2005b). Other inherently gravitationally unstable lakes that have suffered explosive events are Poás (eruptions: 2006–2017) and Rincón de la Vieja (eruptions 2011 - ongoing), both volcanoes in Costa Rica and the extremely acidic crater lake of Kawah Ijen in Indonesia (Lowenstern et al., 2018), which passed through year-long phreatic eruption cycles predominantly characterized by small phreatic eruptions (Rouwet et al., 2010; González et al., 2013). At the crater lakes of Ruapehu and White Island (both in New Zealand), injections of magmatic fluids below a sulphur-sealed vent result in noncyclical phreatic eruptions (Kilgour et al., 2010; Caudron et al., 2018). In Iceland hydrothermal explosions occurred in 2013 when the fluctuating Gengissig ice-dammed lake suddenly drained within the active geothermal area at Kverkfjöll (Montanaro et al., 2016b).

Considering the intense geothermal activity of the area, the known eruption history, a steam-driven, phreatic/hydrothermal eruption is considered as the most likely scenario for future volcanic activity at Boiling Lake (Lindsay et al., 2005a, 2005b). However, due to the relative lack of observations in this remote area, and the paucity of literature, there is a significant lack of understanding of the triggering mechanisms and explosive processes at Boiling Lake. Hazards associated with steam-driven eruptions in similar geothermal settings include ballistic launches of debris and blocks, as well as surges and jets of mud and rocks lacking juvenile components (Browne and Lawless, 2001; Montanaro et al., 2016a, 2016b: Mayer et al., 2015; Strehlow et al., 2017). The absence of reliable precursors of such eruptions (Hurst et al., 2014) further increases their risk potential. Mayer et al. (2017) have recently mapped the distribution of geothermal features in the Valley of Desolation. They highlight how alteration-induced changes in the porosity and permeability of the near-surface environment affect the spatial and temporal distribution of gas and heat emissions. Areas in which permeability reduction occurs can be expected to produce pore pressure enhancement that may result in explosive events (Heap et al., 2017; Mayer et al., 2017; Montanaro et al., 2017). Joseph et al. (2011) investigated the geochemistry of the main geothermal areas of Dominica, whereas further studies have focused on the fluid mechanics of the Boiling Lake (Fournier et al., 2009; Di Napoli et al., 2013) and the composition of the steam flux emanating from the lake. Feuillet et al. (2011) suggested a possible trigger mechanism for the draining process related to the occurrence of large magnitude regional earthquakes. Fournier et al. (2009) developed a conceptual model of the lake system and suggested that drainage events relate to gas influx perturbation, lake geometry and the presence of rocks of differing permeability underneath the lake. The differences in permeability may be due to differences in rock structure and/or hydrothermal alteration (Browne and Lawless, 2001; Mayer et al., 2016; Montanaro et al., 2016a). Hydrothermal sealing of pores and fractures by silica, or other mineral phases is a further mechanism that may reduce the porosity and permeability of the deposits (Mayer et al., 2017; Heap et al., 2017; Montanaro et al., 2017). The hydrothermal alteration of the host rock or of ejecta debris from historic eruptions is, however, only briefly described for the nearby Valley of Desolation (James, 1997; Lindsay et al., 2005b; Mayer et al., 2017), and information on the type of alteration, and its influences on outgassing at Boiling Lake is wholly lacking. Weathering and alteration of steep slopes can favor erosional and mass-wasting processes. In light of this, and similarly to eruptions that have occurred in the Valley of Desolation, explosive events at Boiling Lake may be triggered by landslides from the altered and steep-sided crater-lake walls resulting in blocking the degassing vents. A rapid emplacement of a low permeability landslide body might function as a barrier increasing the overpressure up to values precipitating explosive failure (Mayer et al., 2017).

To estimate potential triggering mechanisms and explosive processes at Boiling Lake we performed field and laboratory measurements using the wall-rocks material representative of the crater lake geology. In particular, we determined how the ongoing alteration affects the petrophysical properties (porosity and permeability) of crater rocks, and in turn how different altered materials can affect ejection behavior during explosive events. To this end, two types of decompression experiment series have been conducted simulating i) a smaller eruption triggered by a drainage event and ii) a more intense hydrothermal eruption due to landslide overburden. Finally, experimental results have been used to calculate ballistic trajectories and to estimate hazard potential within the area of the Boiling Lake.

2. Geological setting

2.1. Dominica

Dominica is located at the center of the Lesser Antilles archipelago between Martinique and Guadeloupe and occupies a land area of 750 km^2 (Lindsay et al., 2005b). The Lesser Antilles are located on a subduction zone where the oceanic crust of the North American Plate is subducted below the Caribbean Plate (DeMets et al., 2000; Maury et al., 1990; Dixon et al., 1998). Dominica has one of the highest concentrations of potentially active volcanoes in the world (up to 9 volcanoes; Lindsay et al., 2003, Lindsay et al., 2005a) and is the most geologically productive volcanic island of the Lesser Antilles since the Miocene (Wadge, 1984). The geothermal activity in Dominica is widespread throughout the island (et al., 2011), and is related to volcanic regions of differing ages. In particular, volcanic activity has shifted over the last 1.6 Ma from the north (e.g. at Morne Diablotin and Morne aux Diable where only low levels of hydrothermal activity remain) to the southern part of the island. Seven major andesitic-dacitic volcanic centers are located in the southern part of Dominica, and are associated with moderate-to-intense geothermal activity (Criaud and Fouillac, 1989), including the highly active areas, Valley of Desolation and Boiling Lake (Joseph et al., 2011).

2.2. Boiling Lake

The Boiling Lake of Dominica is a high-temperature volcanic crater lake, formed after a phreatic or phreatomagmatic explosive event (Di Napoli et al., 2013; Joseph et al., 2011). The lake is situated on a hill east of the Valley of Desolation, 750 m above sea level and 10.5 km away from the capital Roseau (Fig. 1; Fournier et al., 2009). With a water volume of ~1.22×10^4 m^3 when filled (Fournier et al., 2009), the Boiling Lake is the second largest high-temperature lake in the world (Di Napoli et al., 2013). The crater of the Boiling Lake is about 50 m × 60 m in size and 12–15 m deep and boiling appears to be sustained through vigorous upwelling of gases (Fig. 2; Joseph et al., 2011). The dull grey-colored lake surface is surrounded by subvertical walls with a height of approximately 6–30 m (Fig. 2) consisting of block-and-ash debris. A flat area on the northern crater wall, about 13 m above lake level, serves as viewing platform for tourists (Figs. 2 and 3). Fresh water input comes from an inflow and a small waterfall on the north side of the lake. Water also enters the lake via groundwater flow and by steam condensation of hydrothermal fluids. The lake water exits through a crater wall breach on the south lakeside into the Rivière Blanche as well as by evaporation from the surface and draining through the lake floor (see mass balance Fournier et al., 2009). During episodes of heavy rainfall, inflow and outflow remain fairly constant. The lake is

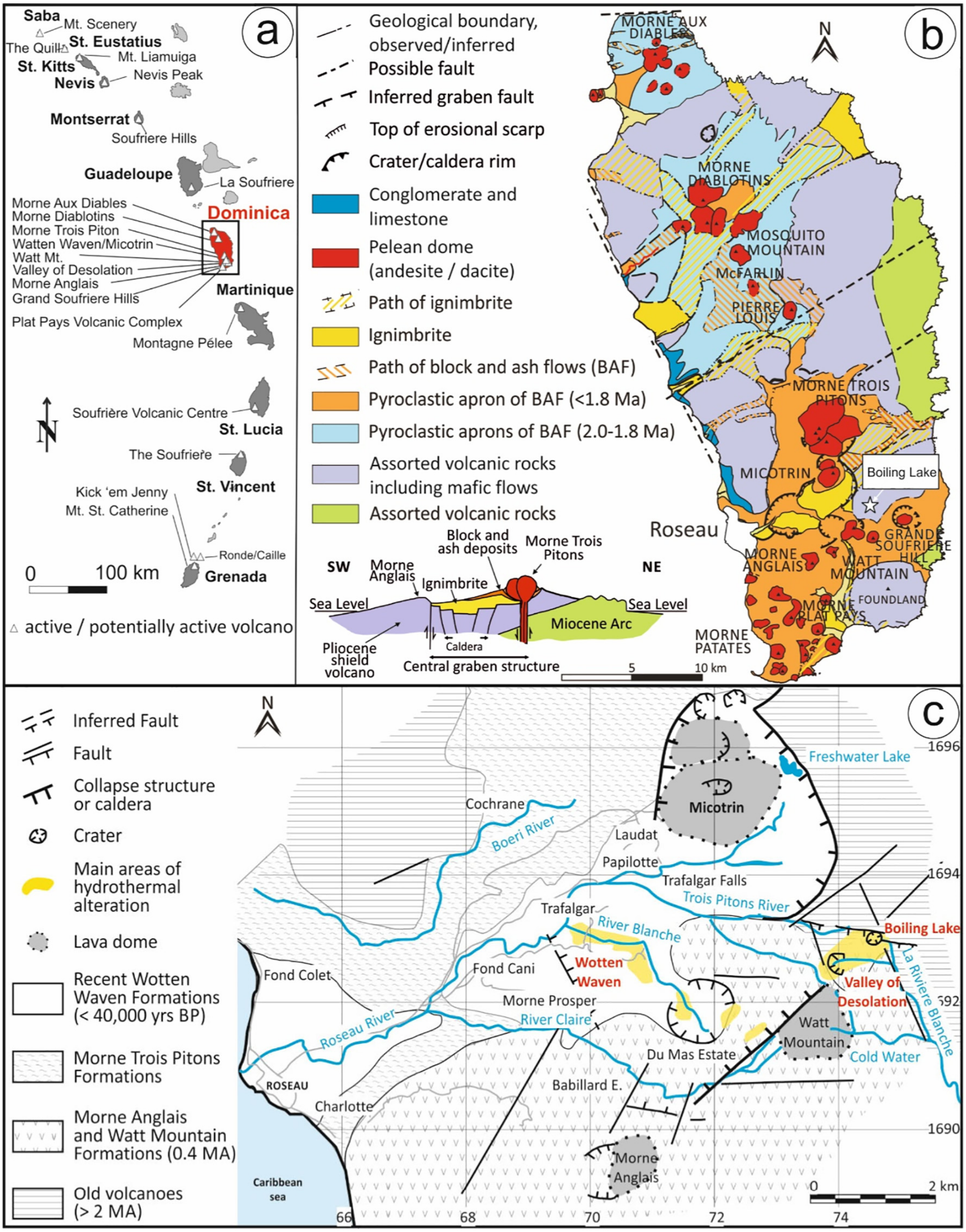

Fig. 1. Overview of Lesser Antilles, Dominica and the hydrothermal areas in the southern part of Dominica (a) Geographical map of island arc of the Lesser Antilles. The island of Dominica is situated between Martinique and Guadeloupe. Modified after Joseph et al. (2011). (b) Simplified geological map of Dominica with a cross section through the island at the height of Morne Trois at lower left. Modified after Smith and Roobal (2004). (c) Geological map of Roseau Valley showing inferred faults, faults, collapse structures or calderas, crater, lava domes and main areas of hydrothermal alteration / activity. Modified after Traineau et al. (2015).

usually in a state of ebullition and the surrounding crater is typically filled with steam clouds and sulfurous vapors. Towards the southeastern part of the lake, an ebullition area/vent, characterized by intense upwelling of water is visible (Fig. 2). The lake activity over the last 150 years has been dominated by long periods of stable water temperature and almost nearly constant fill level ($T = 80$–90 °C, and pH = 4–6) (Joseph et al., 2011; Lindsay et al., 2005b), together with sporadic and rapid sequences of emptying and refilling accompanied by temperature and water chemistry changes (Fournier et al., 2009). During periods of instability, rapid draining down to the local water table (12–15 m) is typically followed by gradual refilling of the lake, along with occasional hydrothermal eruptions and toxic gas emissions which have caused loss of live in the past (Fournier et al., 2009; Lindsay et al., 2005b). During the normal steady state, the lake water is suspended above the local

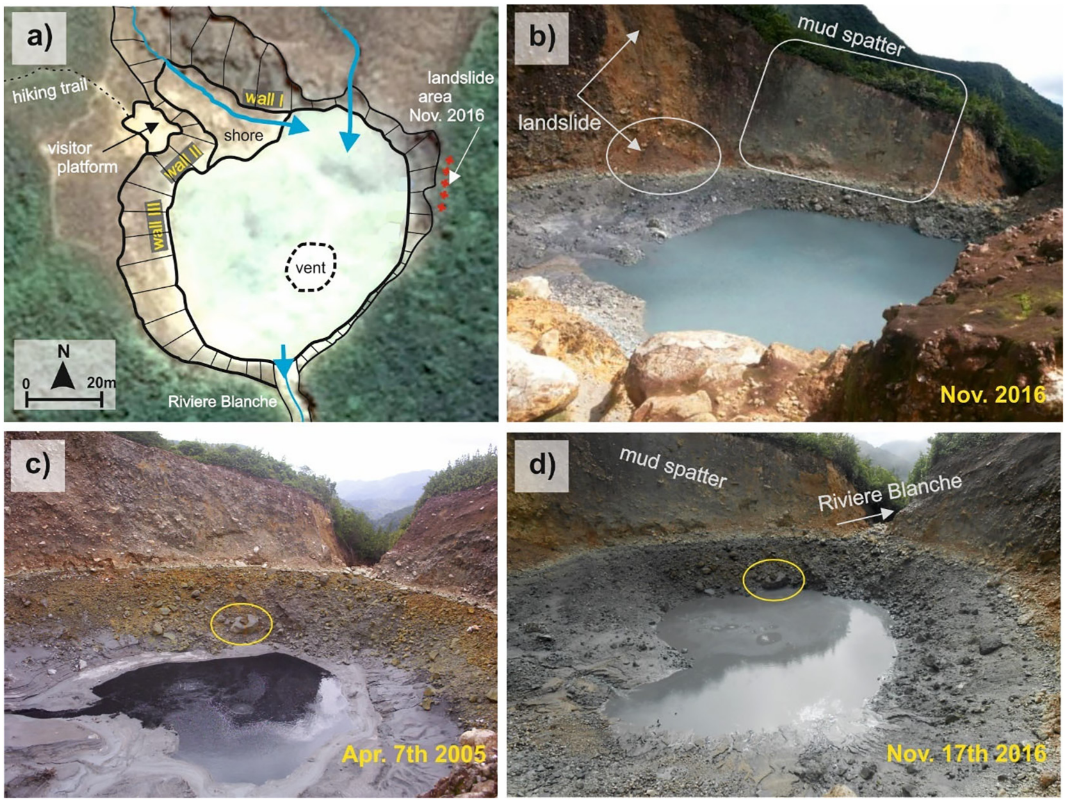

Fig. 2. Boiling Lake (a) Overview, showing the crater, in- and outflow as well as main features of the Boiling Lake. Moreover, the sampled crater wall I – III are marked (backed by google maps image). (b) Boiling Lake in an unstable state, partly filled without boiling activity at the end of 2016. A medium-sized landslide and mud splatter on the flanks of the crater can be seen, where the latter could be the result of a small hydrothermal eruption. Photo was published on Dominica News Online, 6th December 2016. (c) Picture of Arlington James showing the Boiling Lake during a drainage event on April 7, 2005. Only a less lake water, remained in the crater, probably at groundwater level. (d) Photo of the Boiling Lake bed on November 17th 2016 (photo courtesy of S. Durand). For comparison of drainage event 2005 and 2016, an identical boulder is surrounded by a yellow circle near the lake bottom. The increased input of fine clayish sand can be clearly seen in Fig. 2d. This might be the result of landslides from the crater wall and ongoing alteration of wall crater rock. Due to successive input of fine material the steepness of the lake bed flank had changed to a flatter one. The higher water level of the lake compared to 2005 might be the consequence of increased sedimenting which inhibit a further draining of lake water. (For interpretation of the references to colour in this figure legend, the reader is referred to the web version of this article.)

water table by drag forces resulting from a gas phase flowing through a liquid-filled highly permeable conduit (Rouwet and Morrissey, 2015). The boiling of ground water, produced by the presence of a shallow intrusion, continuously supplies rising bubbles. These bubbles condense within the lake providing latent heat for warming up the lake water to approximately 90 °C (Fig. 3). The presence of a low temperature, dense liquid above a high temperature, bubbly, fractured, permeable conduit provides the basis for lake instabilities (Fig. 4; Fournier et al., 2009). Recent geochemical analyses of the Boiling Lake system suggest a deep NaCl brine overlain by a shallow acid sulfate aquifer (Joseph et al., 2019, Fig. 4). The observed irregular drainage events have been inferred to be associated with regional seismic activity favoring shock nucleation of bubbles within the conduit, or to changes in groundwater table levels (Fournier et al., 2009; Feuillet et al., 2011; Joseph et al., 2011). Despite the above, the exact causes for drainage events of the Boiling Lake remain unclear.

Drainage events occurred at least nine times during the past 150 years: 1876, 1887, 1900, 1901, 1971, 1972, 1988, 2004/2005 (Ober, 1880, James, 1988, Fournier et al., 2009) and more recently in November 2016 (Durand, 2016). Some of the total emptying cycles sometimes occurred in periods of <24 h (Fournier et al., 2009; Ober, 1880, James, 2014). The refilling time is in contrast, highly variable, ranging from <24 h through days, to weeks. In 2004/2005 the Boiling Lake drained two times 1) immediately following the 6.3 Mw Les Saintes earthquake and 2) after an associated aftershock (Mw 5.9). Feuillet et al. (2011) proposed that the earthquake generated a volumetric strain increase (expansion) around the lake which in turn contributed to an increase of effective porosity by opening cracks which predisposed the lake to drain rapidly.

As there is no apparent change of temperature or gas/water flux at fumaroles and hot springs in the nearby hydrothermal areas (i.e., in the Valley of Desolation), the process controlling the drastic changes in Boiling Lake seems to be isolated from the surrounding hydrothermal phenomena (Fournier et al., 2009). Monitored fluctuations of the Boiling Lake water level and temperature between December 2004 and April 2005, correlate significantly with changes in water chemistry. The chemical compositional changes during these periods of unstable lake condition indicate a drastic decrease of hydrothermal fluid input into the lake (Joseph et al., 2011).

Turning to the most recent event, the Boiling Lake appeared in a normal state on the 7th November 2016, then drained completely on the 8th of November, leaving a small pool inside the crater. From 8th of November to 1st of December several fluctuations in the water level and degassing activity were observed. By the 15th of December the lake returned to a “normal” (and stable) level and activity. A survey of the lake on 8th of November revealed the presence of mud splatter on the crater wall and its above growing vegetation (Durand, 2017, Fig. 2). This latter element would suggest that the drainage event was accompanied by a small mud-rich explosive event. Interestingly, a small landslide from the eastern crater wall of the Boiling Lake took place several weeks (between May and November 2016) prior to the actual draining events.

Previous studies investigated the chemistry of the lake water (Joseph et al., 2011), characterized the emitted gases (Di Napoli et al.,

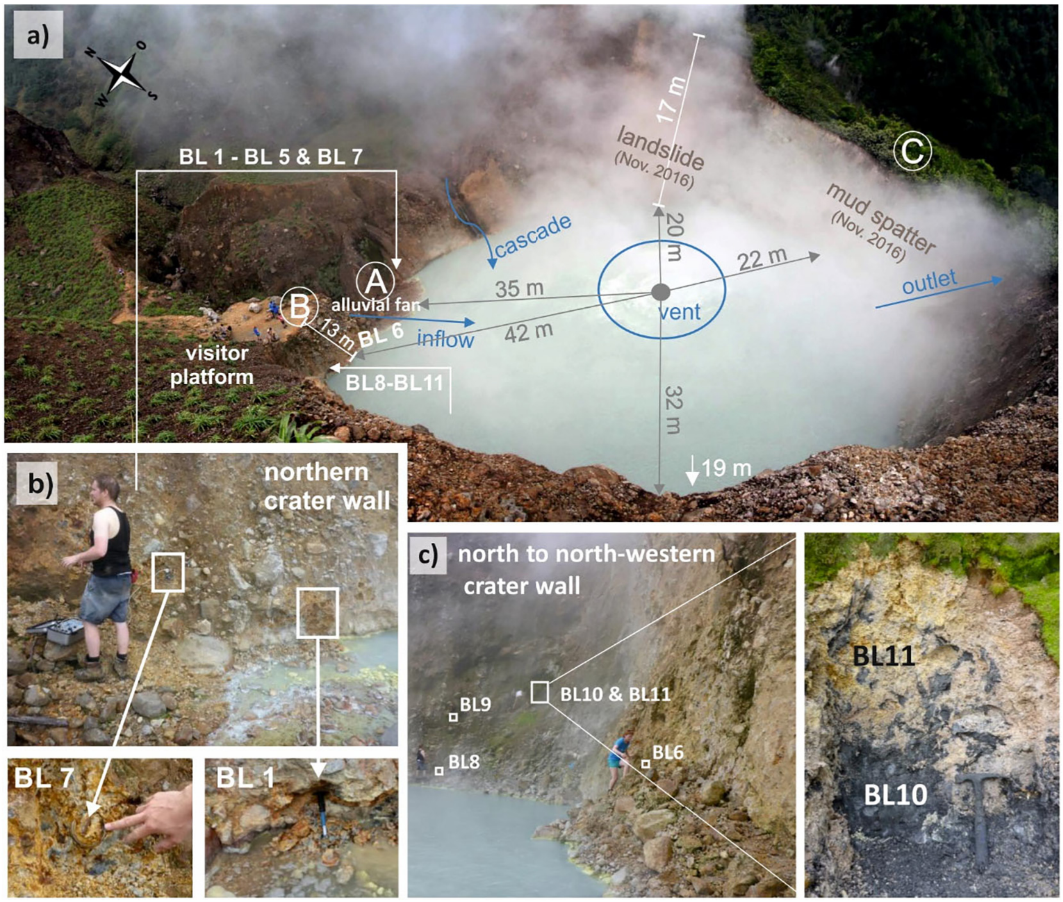

Fig. 3. Geometry of the Boiling Lake crater and sample locations (a) The photograph (from May 2015) shows the view from the west crater wall down to the lake. Steam and vapor come from the lake surface and fill the crater. From the north direction, a cold stream flow over an alluvial fan (point A) into the lake. A small cascade supplies water from the eastern side. Towards the south-eastern side of the lake, a point of upwelling water (vent) is located. On this point the water is elevated a bit above the general water surface. An outflow into the Blanche River breaks through the southern crater wall. On the northern side a visitor platform (B) allows a nice view on Boiling Lake for visitors. Point C on the eastern crater wall marks the place where vegetation was probably affected by a hydrothermal eruption in Nov. 2016. (b) Sample location of BL1 and BL7 on the northern crater wall (wall I), left (view towards the lake) of the alluvial fan (c) BL6 was taken on the northern crater wall (wall II), beneath the visitor platform on the right side (view towards the lake) of the alluvial fan. BL8 to BL11 were excavated at the north-western wall (wall III). (See people for scale).

2013), as well as allowed to develop a conceptual model of the Boiling Lake system and its drainage events (Fournier et al., 2009). However, little or no information is available regarding the lithology of the crater wall, and of the lake floor itself. Thus, we are missing fundamental parameters like rock strength, porosity or permeability which highly affect the rock resistance and which are fundamental to understand possible trigger mechanisms of eruptions in such a hydrothermally-active environment (Montanaro et al., 2016b; Mayer et al., 2017; Heap et al., 2017).

3. Investigated sites and methods

The lithologies of the crater were characterized and sampled during two field campaigns carried out at the Boiling Lake in April 2013 and May 2015. The investigated sites were the only ones safely accessible, yet are considered representative of the materials making up the crater walls surrounding the lake. The lithologies consist mainly of mildly consolidated, and heterogeneous block-and-ash flow deposits (Fig. 2). Samples were collected at three different crater wall locations, all near the outcropping lake floor. In particular, material was taken from the wall (Figs. 3) namely: i) the northern part of the crater (wall I), left of the alluvial fan (BL1 & BL7), ii) the northern crater wall beneath the visitor platform (wall II) and on the right of the alluvial fan (BL6), and iii) the northwestern crater wall (wall III; BL8, BL9, BL10, BL11).

Slightly consolidated material (BL6 – BL11) was sampled using coring with steel cylinders (length = 61 mm; diameter = 72 mm), which were plastic-wrapped and sealed with tape to avoid any loss of moisture or destruction of original rock texture. To obtain fresh samples of the wall rock, the steel cylinders were pressed into the respective wall after removing a minimum of 5 cm overlying rock. Material at location BL1 was instead removed with a spade and stored in plastic boxes. At location BL7, several centimeter-sized consolidated clasts, representative to the coarse fraction of the deposit, were also sampled (BL7_T1, T2, T3; Suppl. mat. Fig. A.3).

Besides samples BL2 to BL5 and BL7, all remaining samples were used for further petrophysical, grain size and geochemical characterization.

3.1. Field-based characterization of crater wall-rock

Punctual measurements of permeability and moisture content of unconsolidated material representative of the circum-crater variation in the wall types at the Boiling Lake crater walls were taken by using a PL-300 soil permeameter (Suppl. mat. Fig. A.2; Umwelt-Geräte-Technik; Heap et al., 2017; Mayer et al., 2017; Montanaro et al., 2017). Cylinders containing the samples for laboratory investigations were weighed to determine bulk density. Selected samples were immediately sealed and wrapped for transport. This technique allowed non-destructive sampling and preservation of sample texture and water content required for further analysis in the laboratory.

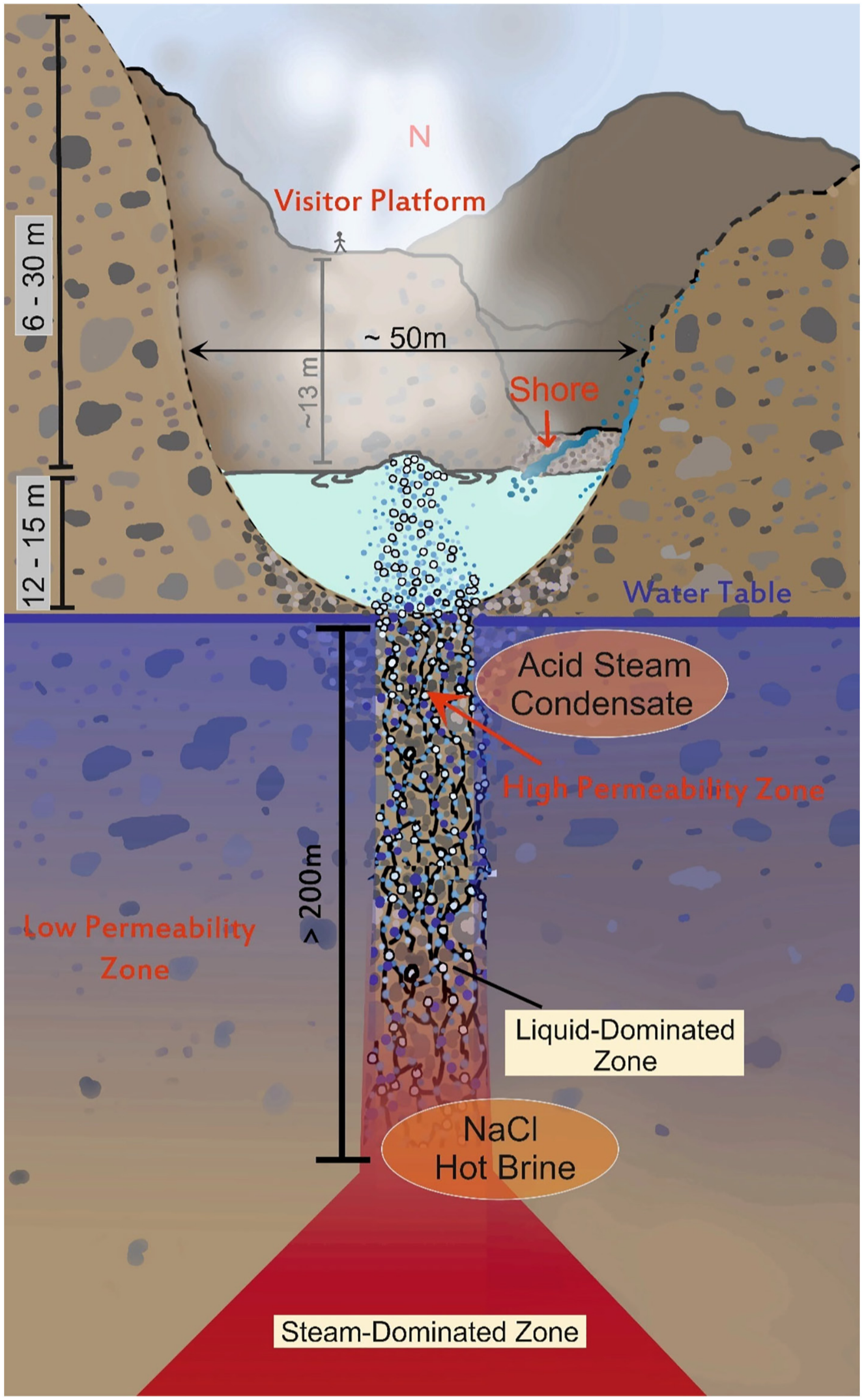

Fig. 4. Conceptual model of the Boiling Lake with view towards the north direction. A flat area on the north crater wall, about 13 m above the lake represents a viewing platform for tourists. A small cascade supplies water from the eastern side of the lake. The crater is filled with steam and sulfurous vapors coming from the lake surface. An area of upwelling water and gas is located at the south-eastern side of the lake (situated above the vent). The rock material of the crater wall consists of unconsolidated to slightly consolidated block and ash flow. The volcanic lake is suspended above the local water table by drag force and buoyancy caused by a gas phase flowing through a liquid filled high permeable conduit (Rouwet and Morrissey, 2015). The constant supply of rising bubbles comes from the boiling groundwater near an intrusion. Fluid chemistry made by Joseph et al. (2019) suggests a shallower acid-sulphate hydrothermal aquifer and a deeply sourced NaCl brine.

The field characterization of the investigated unconsolidated material additionally involved two hand-held devices: a pocket penetrometer that allowed measurements of the unconfined compressive strength (Zimbone et al., 1996), and a torvain used to measure the undrained shear strength (Farquhar, 2001).

All samples petrophysical and mechanical properties were obtained well within the measurement range of the applied instruments (Table 1). It should be noted that despite the fact that the field methods used provide valuable estimates for permeability and rock strength, their accuracy and precision are often not comparable with well-

Table 1
Photographs of cored samples from slightly consolidated crater wall material of the Boiling Lake (diameter 72 mm). Below a table of petrophysical properties determined in the field and in the laboratory is shown where ρ_b = in situ bulk density; ρ_m = dry matrix density; φ = connected porosity; k = in situ gas permeability measure with PL-300; $m_{in\ situ}$ = in situ volumetric moisture measured with PL-300; m_{lab} = volumetric moisture measured by oven drying; Cs = unconfined compressive strength; Ss = undrained shear strength. – Not intended because material from BL7 was not taken to the laboratory.

	BL6	BL7	BL8	BL9	BL10	BL11
ρ_b (g/cm^3)	1.82	1.66	1.08	1.68	1.73	1.49
ρ_m (g/cm^3)	2.70	-	2.57	2.66	2.73	2.80
ϕ (%)	30.9	-	66.3	48.2	56.9	56.5
k (x 10^{-15}m^2)	2.27	-	8.31	1.13	0.76	1.79
$m_{in\ situ}$ (vol%)	34.6	75.4	61.1	52.8	100	100
m_{lab} (vol%)	31.8	-	57.6	48.2	61.2	81.0
Cs (kN/m^2)	4.3	5.0	3.4	5.0	3.4	2.5
Ss (kN/m^2)	1.8	2.5	2.2	3.8	2.2	1.8

constrained laboratory methods (Heap et al., 2017). However, such measurements remain extremely valuable for being the first characterization of petrophysical and mechanical properties of rocks at Boiling Lake.

3.2. Laboratory-based characterization of sampled material

3.2.1. Geochemical and mineralogical analysis

The bulk chemical composition of each sample was determined by wavelength dispersive X- ray fluorescence (WD-XRF) analysis on bulk samples. Geochemical data, together with mineralogical analyses conducted by optical microscopy, was further employed to determine the type and degree of alteration. The relationship between chemical variation and alteration was evaluated using five indices, as proposed for characterization of the degree of alteration in different lithologies (see Pola et al., 2012 and references therein). These indices, which are based on the weight percent ratio of major elements, assume that distribution of chemical elements is controlled by the degree of alteration (Duzgoren-Aydin et al., 2002). Details of sample preparation and analysis, as well as alteration index calculations are reported in the Supplementary material.

3.2.2. Petrophysical characterization, grain size analyses, and componentry

Soil samples were further characterized in the laboratory to determine their rock physical properties. Samples were dried in an oven at 65 °C for at least 24 h until fully dry. Weighing of samples prior and post drying allowed the mass determination of dry sample material and water and therefore the volumetric moisture (Table 1) which can be compared with moisture measured in the field. Dry powder density of all samples was obtained by helium pycnometry (Ultrapyc 1200e®, Quantachrome). Knowledge of the volume of the sampling cylinder, as well as the water content and dry density, enabled determination of

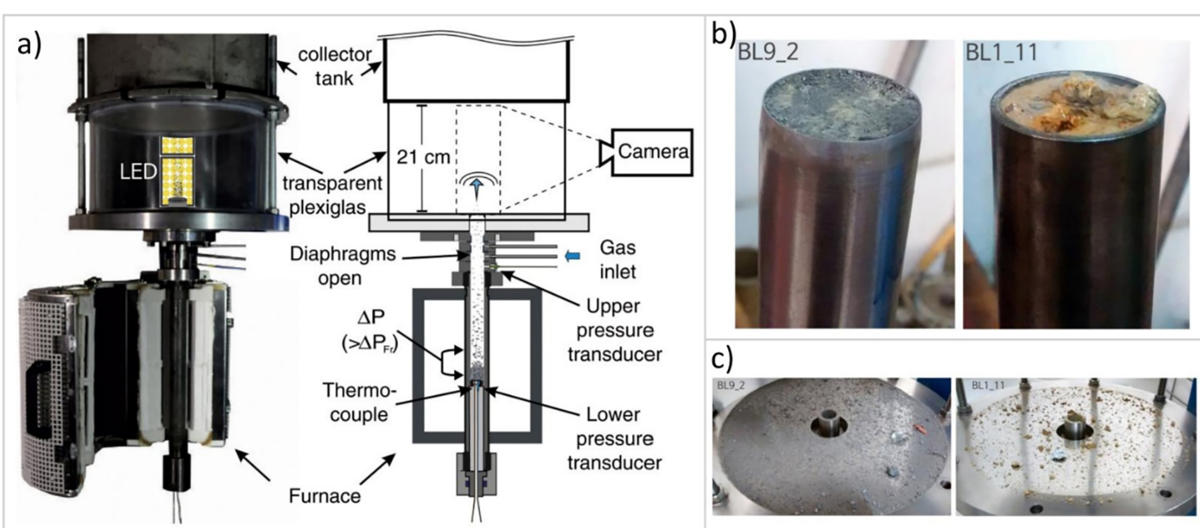

Fig. 5. Experimental setup (a) Fragmentation bomb at LMU Munich (modified after Mayer et al., 2015). The setup is divided into two sections. On the top of the installation is a low pressure tank with a transparent Plexiglas® part on the bottom, where ejected particles can be collected and recorded with a high-speed camera. The ejection scene is illuminated with LED's from behind. The high pressure and high temperature section is situated at the lower part and consists of an autoclave in which the sample is mounted. The autoclave is heated externally and pressurized by argon gas. At the bottom of the sample a dynamic pressure sensor and a thermocouple is located. (b) Sample holder with rock material from decompression experiments. For BL9_2 crater wall material with original texture and water content is used. For BL1_11 the sample holder is filled up with loose sample material and distilled water. (c) Bottom of low pressure tank after decompression experiment. The ejected material of BL9_2 (Setup 2) is almost dry and finely dispersed. The rock fragments of BL1_11 (Setup 1) is partly agglomerated and wet.

the porosities of the samples, which is a key parameter controlling their mechanical behavior (Pola et al., 2014; Mayer et al., 2016; Heap et al., 2017).

Grain size distribution analyses of the sampled material were carried out by dry-sieving of particles between 16 mm and 63 μm, whereas laser refraction techniques, using a Coulter LS230 (measuring range 0.375–2000 μm, wave length 750 μm) were used to analyze the fraction below 63 μm.

The particles of different sieve fraction were also analyzed petrographically in order to characterize their colour, degree of alteration, and mineral content.

3.2.3. Rapid decompression experiments

We conducted decompression experiments with the "fragmentation bomb" apparatus at LMU (Fig. 5a), described in detail by Alidibirov and Dingwell (1996) and developed further by e.g. Scheu et al. (2006), Alatorre-Ibargüengoitia et al. (2010); Rager et al. (2014); Mayer et al. (2015). The apparatus consists of a large upper chamber operating at ambient pressure and temperature conditions, and a smaller high-pressure chamber (autoclave) which is heated and pressurized, usually by Argon gas. The autoclave is separated from the chamber by a series of diaphragms. Controlled rupturing of the diaphragms initiates rapid decompression of the autoclave. A transparent section at the bottom of the large chamber allows monitoring of the sample ejection using a high-speed camera.

Unconsolidated samples collected in larger cylinders from the wall of the Boiling Lake (Section 3) were "cored" using smaller cylinder fitting the autoclave size; grain size analyses of residual material from the large cylinder, and material from the smaller ones show the same grain size distribution. This assured that the exploded samples were representative of the original soil sample. The experimental conditions of pressure and temperature, were chosen to best mimic two type of scenarios triggering explosive events (Figs. 5 and 6): i) a lake drainage, and ii) a partially burial by a landslide body.

In the first scenario (Setup 1) we assume a lake drainage associated with a decrease in hydrothermal activity, and thus in fluids (and heat) supply (Joseph et al., 2011). During drainage a drastic decrease of hydrothermal/magmatic fluid input into the lake occurs (e.g. caused by changes in fluid flow or disturbance of fluid pathways in permeable region). Such a decrease of fluid input likely disturbs the intrinsically unstable system formed by a dense liquid lake atop a gas- or multiphase-filled conduit (Fournier et al., 2009; Vandemeulebrouck et al., 2005). A mixture of water and a considerable amount of suspended material (mud, silt and sand) flow down into the highly permeable conduit causing the plugging of the vent zone and a cooling of the high permeable region. Once the conduit heats up again, thus returning to its "normal conditions", water starts to boil and, together with the steam produced, attempts to percolate through the plugged vent and refill the crater lake. Depending on the permeability of the plugged zone, this can lead to the accumulation of superheated water and non-condensable gases, and thus in pressurization below the plugged area (Hurwitz et al., 2016; Montanaro et al., 2016b). Looking at drainage and refilling events in the past, the emptying or backfilling process of a certain amount of lake water can last from 75 min (e.g. in 1900) to 37 days (e.g. in March 2005 refill from 8 m below the outlet to almost normal level lake level; James, 2005). Assuming a vent cross section of about 7 m^2, and considering the lake-refilling time range, the formation of a sediment "plug" 1-to-10 m thick with a permeability lower than 10^{-12} m^2 would be enough to produce over-pressurized conditions. The explosive liberation of a plugged vent under the above assumed conditions will require only low pressures in the order of 2–3 bar. This pressure range is selected due to the combination of lithostatic, hydrostatic (remaining lake water) and vapor pressure. To satisfy the condition of maintaining the water at liquid state before and during the re-heating of the system, together with pressures consistent with the above, a temperature of 120 °C is assumed below the plugged area (Fig. 7). For this kind of experiment, loose sampled material fully saturated with water was carefully placed into sample holders (Fig. 5b).

The second experimental series (Setup 2) simulates an eruption triggered by a landslide body that partially fills the crater and blocks the vent (Fig. 6). Here we assume that the vent area is overlaid by max. 10 m of material sliding from the steep crater wall, having a relatively low permeability in the order of 10^{-15} to 10^{-16} m^2 or marginally above

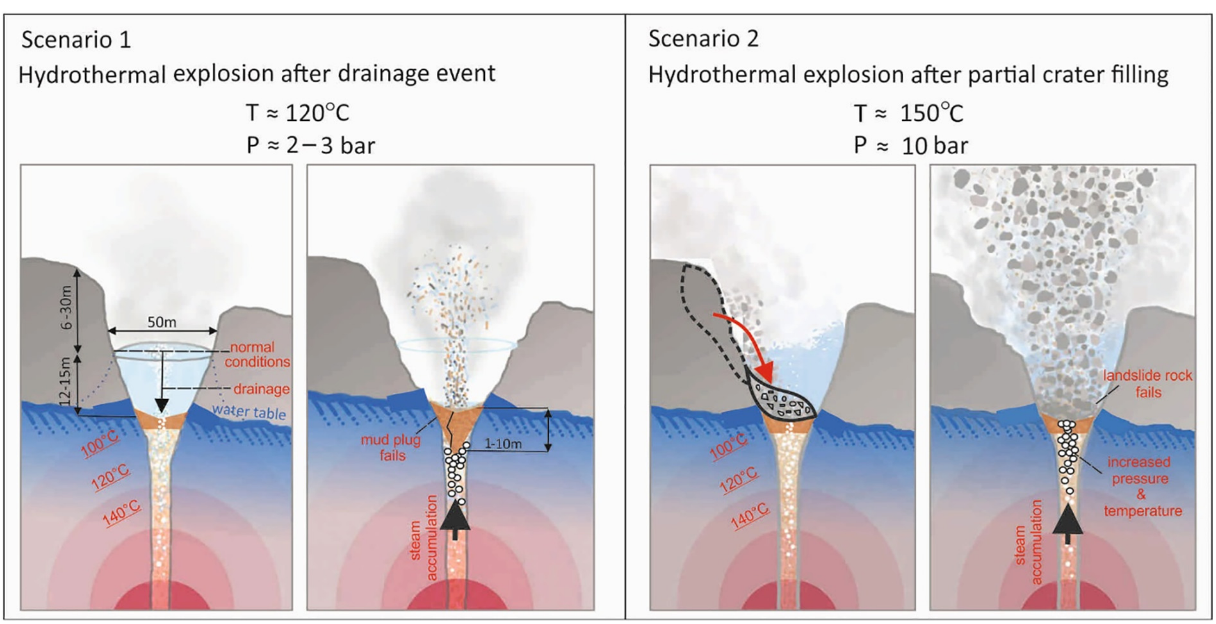

Fig. 6. Two experimental setups: Scenario 1 shows a small hydrothermal eruption after a drainage event. Due to disturbance in hydrothermal system, the lake drained until the local water table. Suspended material blocks the highly permeable vent. A pressure build-up follows after reactivation of the hydrothermal system and ends in a hydrothermal eruption. For this setup and a rock density of about 2.6 g/cm^3 a pressure range between 2 bar and 3 bar and a temperature of approximately 120 °C is used for decompression experiments. Scenario 2 illustrates a hydrothermal eruption during excavation of the Boiling Lake. In this setup, we assumed that the crater lake is partly or fulfilled with rock material due to landslide. To overcome lithostatic pressure a pressure of approximately 10 bar and a temperature of about 150 °C is used for experimental setting.

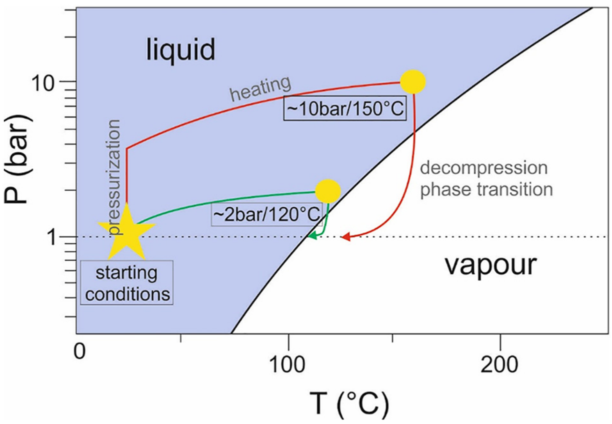

Fig. 7. Phase diagram of water with heating and pressurization process of the two decompression setups. The installation is pressurized until a certain pressure, then a furnace starts the heating procedure which leads to a further increasing of pressure. When the final P/T conditions are reached, the system is flooded with argon gas which leads to a rupturing of diaphragms and fast decompression. Due to decompression, a phase transition from liquid water to vapor phase occurs. Setup 1 (drainage event) is marked by the green path, Setup 2 (landslide event) by the red path. (For interpretation of the references to colour in this figure legend, the reader is referred to the web version of this article.)

(in similarity to the in situ permeability measured at the crater wall - see section below). Even if a small landslide is produced to partially cover the vent area, and the degassing through the free part of the vent persists, a slow but continuous pressurization at the bottom of the landslide body can be expected. Depending on body thickness (10 m) and permeability we evaluated, based on Darcian flow, that a period of several weeks to even years would be needed for the gas to percolate through the landslide body. In this period, the accumulation of steam and gas below a low permeability cover can result in the uplift of the overlying material, and may cause “fractures” in the landslide body allowing for rapid degassing, and in turn for the flashing of hot, and pressurized liquids (Mayer et al., 2017). If fracturing and degassing are not occurring, the landslide “cap” will eventually fail once a critical pressurization from below is reached. This critical pressure depends on the thickness of the landslide body, its density/weight (overburden) and its cohesion. Mayer et al. (2017) investigated a similar scenario, based on an explosive event, which occurred in 1997 at the nearby Valley of Desolation and produced the burial of the fumarolic vents by a 2.5–3 m thick landslide body. Analytical modeling of hydrothermal altered samples and decompression experiments together with ballistic observations of erupted material from 1997, suggest that overpressure of 3–5 bar would suffice to produce an eruption at such site. A similar triggering process for steam-driven eruptions was observed at Geysers Valley in Kronotsky Nature Reserve in Kamchatka in 2007. Here, an enormous landslide unevenly covered fumarolic fields, at some sites >20 m-thick, which lead to overpressure conditions and explosive blasts (Kiryukhin et al., 2012).

In our scenario, considering a landslide body 10 m thick having a strength/density as measured in situ and in the lab (see Section 4.2), failure conditions are estimated to be reached for pressures up to 10 bar. We decided for the previously mentioned pressure range, to use lithostatic and hydrostatic (remaining lake water) pressure combined with vapor pressure with respect to overpressure conditions used in the “landslide event” of Valley of Desolation experiments. The pressure may be slightly overestimated to ensure an entire ejection of landslide rock and to propose a maximum hazard zone. It is also reasonable to consider an increase in temperature with pressurization, following the boiling curve, which would result in a pre-explosive temperature of about 150 °C. For this kind of experiment, sampled material with original rock texture was placed into sample holders and mounted into the autoclave without adding any water, thus representing the original moisture of the sample (Fig. 5b). Only for decompression experiments BL7_1 and BL7_2 the sample holder was filled with loose material from location BL1 and filled with a similar amount of water which can be found in the original crater wall rock.

During the experiments, the decompression results in the explosive boiling of the water (and the formation of steam respectively), which drives the eruption and is the same process invoked for both the simulated scenarios. During these experiments the entire pressurization, heating and dwelling process lasted 20–30 min, ensuring the samples reached thermal equilibrium.

In both type of experiments, high-speed video analysis allowed the determination of ejection velocities for particles of differing sample size, while the ejected material was recovered and analyzed for its grain-size distribution. Grain-size of experimentally-disrupted material was then compared to the sample's initial size distribution. Thus, experiments allowed us to qualitatively investigate the role of the used lithologies, and of their natural texture and grain size, on the “fragmentation” and ejection dynamics of the eruptions.

3.2.4. Ballistic modeling and application to eruption scenarios

To estimate the effects of hydrothermal explosive events in respect to the investigated scenarios at the Boiling Lake, theoretical ballistic trajectory distances were calculated. For this approach, ejected particles were treated as ballistic projectiles (Mastin, 1995). Ejection velocity and particle size, which were obtained by high-speed video analysis, as well as particle (bulk) density as determined during the rock physical characterization, were used as input parameters. The ballistic trajectories were then calculated using the Eject! software of Mastin (2001). By assuming a spherical particle shape, ejection angles of 45° and 65°, and neglecting wind direction and speed, maximum trajectory distances could be estimated. The incorporated variable drag coefficient that evolves as the Reynold number of the projectile evolves (Wadsworth et al., 2018) were used for our ballistic modeling. Calculations allowed us to analyze the influence of particle size in the range of lapilli (2–8 mm) on their trajectory distances.

4. Results

4.1. Field results

The material at Boiling Lake was mostly sampled on the (accessible) northern-northwestern sectors, and it is representative of the outcropping lithology around the crater lake (Fig. 3). The collected ash and block flow material mostly consists of mildly consolidated breccia with different degrees of alteration, colors, and clay content. In general, all samples show relatively low permeabilities (Table 1), with the lowest values measured for materials sampled from the northwest wall (BL9 and BL10 from wall III). Nevertheless, a rather low pH of 5 (measured on the rim of the Boiling Lake with pH measuring strips), high humidity, and high sulphur contents of rock samples, give rise to uncertainties in the permeability and moisture measurements, which are difficult to quantify.

In particular, at the location wall I (BL1 and BL7; Fig. 3b), the deposits consist of slightly consolidated breccia with ochre colored matrix and fragments up to several centimeters in size (e.g. type 1, 2, 3 described below). The breccia in its more consolidated part is hard in its consistency (5 kN/m^2), and has a moisture content of 75.4% (Table 1). At the location wall II (BL6; Fig. 3c), the deposit consists mostly of a dark, clay-rich matrix that appears hard and brittle, and contains large clasts (up to several centimeter). Reddish-brown oxidation crust are covering the deposit in this sector. The sample material from such lithology showed a low permeability (2.26×10^{-15} m^2) and a low moisture content of approximately 34.6% as well as a hard consistency (4.3 kN/m^2) (Table 1). At the wall III location, the deposits in this section (BL8, BL9, BL10; Fig. 3c) are made of medium grey, clay-rich material intercalated with a few sulfurous layers. The fine-grained material contains scattered centimeter-large soft clasts inside the matrix. In the upper section of the wall (BL11; Fig. 3c) the surficial deposit appears yellow/ochre in colour with brown streaks, and seems to be representative of a strongly-altered variety of the material in the inner part of the crater wall (BL10). This material is particularly visible at the surface of the wall or next to cleavages. Overall, lithologies at the western wall are characterized, from the base to the top, by a decrease in permeability (8.29×10^{-15} to 7.5×10^{-16} m^2), associated to an increase of moisture content (61 to 100%), and decrease in consistency (5 to 2.5 kN/m^2) and shear resistance (3.8 to 1.8 kN/m^2).

4.2. Laboratory results

4.2.1. Geochemical quantification of alteration

As a result of geochemical analysis (Suppl. mat. Table A.1), most of the sampled material showed dacitic composition and a variable range of alteration, as confirmed by calculated alteration indices (Section 3.2.1). CIA (Chemical Index of Alteration), PIA (Plagioclase Index of Alteration), and CIW (Chemical Index of Weathering) values generally rise due to the loss of mobile cations within facies with hydrothermal and supergene alteration. These indices correlate well with the increase in the degree of alteration (e.g. CIA of 76.71 and CIW of 83.65 for the highly fragile and altered crater wall III sample BL11) observed in the investigated samples (Table 3). However, these indices must be applied with caution to heterogeneous samples from highly hydrothermally active environments, since their estimation assume immobility of aluminum (Arikan et al., 2007; Pola et al., 2012). Despite the uncertainties, an increase in the effect of both alteration types can be observed going from the northern wall to the northwestern side, with sample material of crater wall III showing highest values for these parameters (Table 3). By contrast, the SA value decreases with alteration as it reflects the loss of silica.

4.2.2. Mineralogical composition

We analyzed four rock lithotypes representative of the main components found in the Boiling Lake crater wall deposits. Lithotypes 1 to 3 were collected from the northern wall I, next to BL1 (Fig. 3a, b, and Suppl. mat. Fig. A.3), while lithotype 4 was taken from the northwestern crater wall III next to BL10 (Fig. 3c and Suppl. mat. Fig. A.4). In thin section all samples show porphyritic texture with larger crystals suspended in a dense matrix (Fig. 8 and Suppl. mat. Fig. A.8). Lithotypes collected from crater wall I can be divided into a white-grey, dark grey and a red to violet clast variety containing predominantly amphiboles, pyroxenes, plagioclases and sometimes quartz embedded in a fine groundmass. Crater wall III almost contains medium grey lithotypes containing plagioclase, clinopyroxenes amphiboles embedded within a crystalline groundmass (more detailed description in supplementary material).

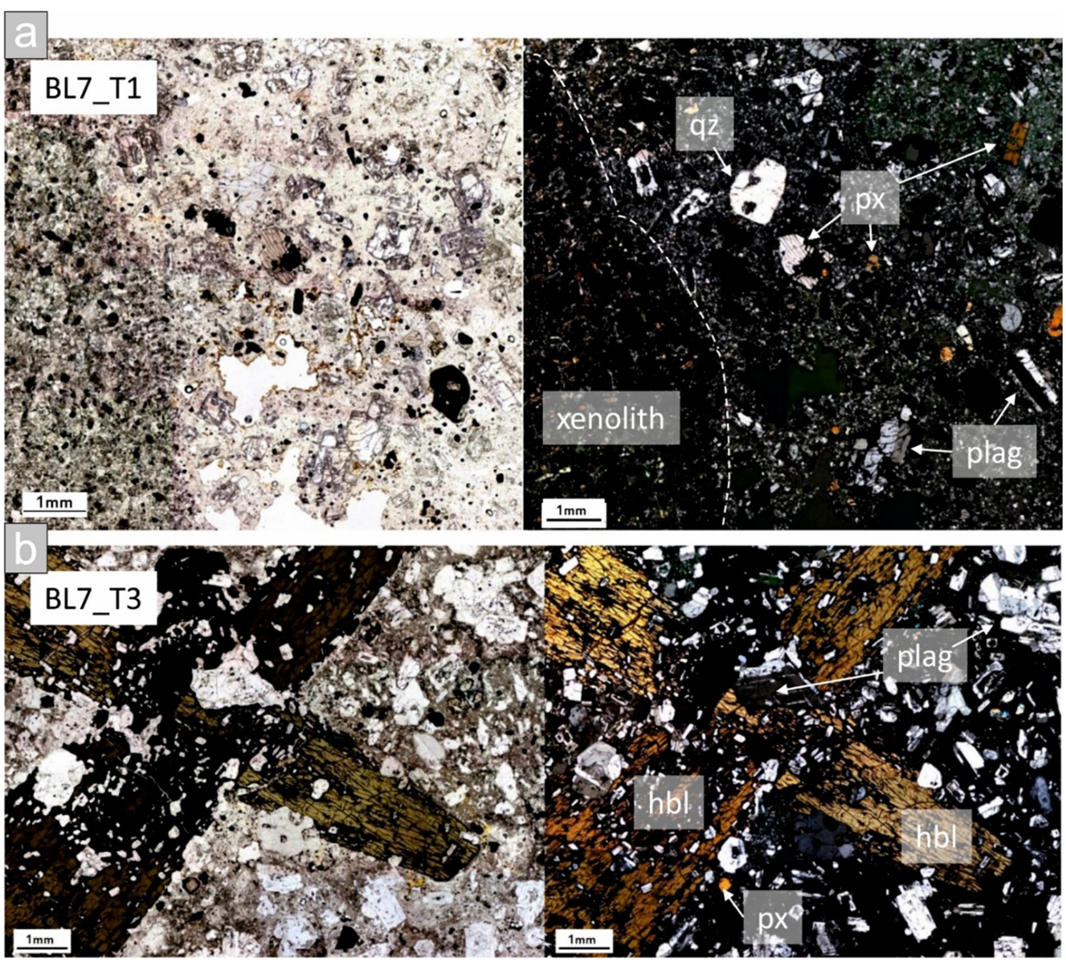

Fig. 8. Thin section of BL7_T1 (top) and BL7_T3 (bottom) without analysator (left) and with analysator (right). Both were sampled at crater wall I. BL7_T1 contains a xenolithe which has another texture than the rest. The minerals of the rounded xenolithe are nearly equal sized. It contains predominantly pyroxene, plagioclase and a large number of opaque minerals. The rest of the thin section has a porphyritic texture. The major minerals are plagioclase, pyroxene and rounded quartz. BL7_T3 contains large amphiboles (hornblende) with strong pleochroism. This thin section has more large minerals and the matrix is much finer, compared to the other samples. Pyroxene, rounded quartz and a high amount of zoned plagioclase are also visible. (qz = quartz; hbl = hornblende; plag = plagioclase; px = pyroxene).

Table 2
Experimental conditions and results. Note: For realistic ballistic calculation BL7_2 and BL9_4 should not be considered because decompression rates over 10 bar would involve an unrealistic large landslide-rock-capping. Nevertheless, the results of these two experiments reveal interesting insights, justifying their inclusion in this table.

Sample	P	T	m_{H2O}	m_{solid}	E_{vol}	E_{mass}	$v_{eject\ front}$	$d_{max\text{-}hor\ 45°}$	$d_{max\text{-}ver\ 45°}$	$d_{max\text{-}hor\ 65°}$	$d_{max\text{-}ver\ 65°}$
	(bar)	(°C)	(g)	(g)	(MJ/m³)	(J/g)	(m/s)	(m)	(m)	(m)	(m)
lower P/T experiments (Setup 1)											
BL1_11	2.2	115	13.0	30.16	2.4	5.2	22 (±2)	34.3	10.6	25.6	16.4
BL1_12	3.2	120	14.0	30.51	3.5	6.9	59 (±4)	33.3	14.4	23.7	20.7
BL5_5	2.8	113	14.0	28.85	2.1	4.5	39 (±3)	23.8	8.6	17.6	12.6
BL5_6	2.8	110	13.0	30.43	1.5	3.5	54 (±5)	27.9	11.0	19.6	16.5
higher P/T experiments (Setup 2)											
BL6	10.0	152	8.7	57.42	5.0	17.7	102 (±4)	61.6	28.1	42.8	39.9
BL7_1	9.9	152	12.5	49.98	8.0	17.7	97 (±6)	95.4	38.5	68.0	57.3
BL7_2	15.5	158	6.1	54.78	4.3	19.6	89 (±5)	67.0	27.2	47.3	40.5
BL8	10.8	155	12.4	26.26	7.6	18.7	128 (±6)	70.7	33.1	49.6	47.4
BL9_2	10.2	154	11.9	42.50	7.1	18.4	104 (±6)	58.8	28.1	40.5	40.7
BL9_4	13.3	162	11.3	40.41	7.7	21.0	132 (±6)	69.2	32.4	48.0	47.2
BL10	10.3	155	14.1	39.60	8.7	18.7	116 (±6)	51.9	23.7	35.3	34.1
BL11	10.1	152	17.1	34.40	10.2	18.0	118 (±4)	49.2	26.5	31.5	36.1

4.2.3. Petrophysical properties, grain size distribution and clast nature

Petrophysical sample properties and grain size determined in the laboratory are provided in Tables 1, 2 and Fig. 10. In-situ moisture content of unconsolidated samples range from 34.6 to 100 vol% and was higher than the water content determined in the laboratory by drying (31.8 vol%–81.0 vol%). The differences probably originate from sample heterogeneities and the loss of water during sample shipping. During transport samples were possibly exposed to significant temperature and pressure changes that likely induced changes in water distribution within the sample cylinders.

The dry matrix density is quite similar for all of the collected samples and ranges from 2570 to 2800 kg/m^3, while the bulk density varies between 1080 and 1820 kg/m^3. Permeabilities of different crater walls are quite low and cover a narrow range of 8.31×10^{-15} to 0.76×10^{-15} m^2. In contrast, they show a wide range of porosity from 30.9% at wall II location to values ranging between 48.2 and 66.3% at wall III (Table 1).

Material collected at different locations around the lake show a variation in the grainsize distribution. Sieving analysis of original crater wall samples shows poorly-sorted gravelly sand with fines for BL1 (wall I) and BL8 (wall III) and moderately well-sorted gravelly sand with fines for BL6 (wall II), BL9, BL10 and BL11 (wall III). In general, samples from the crater wall I (BL1, BL5 & BL7) appear to be more heterogeneous and contain larger clasts (mode = 1.4 mm, median = 1 mm) compared to the other samples. One exception is the grainsize of BL8 sampled at the bottom of wall III, approx. 0.5 m above the lake surface which is very heterogeneous resulting in the highest mode (2 mm) and median (1.4 mm). Wall II and wall III samples are similar in mode (0.18 mm) and mean (0.25 mm). BL11 from wall III contains the largest amount (0.2 wt%) of fine particles <4 μm (Fig. 10 and Suppl. mat. Fig. A.6).

A closer look into componentry of grain types shows clear differences between the crater wall materials. An overview is reported in the Suppl. mat. Fig. A.7. In general grain types from wall III seem to be more affected by alteration compared to crater wall I and II containing very fragile components and crusts sometimes completely made of sulphur (e.g. BL8 type 3).

Table 3
Based on geochemical analysis, indices used to estimate the degree of alteration were calculated. Chemical index of alteration (CIA), the plagioclase index of alteration (PIA), the chemical index of weathering (CIW), the alumina to calcium sodium oxide ration (ACN), the silica to alumina ration (SA) and the alumina to potassium sodium oxide ratio (AKN).

Sample	CIA	ACN	SA	AKN	PIA	CIW
BL6	69.54	0.81	3.50	3.09	55.62	80.78
BL7	63.01	0.67	4.14	3.44	56.59	67.32
BL7_T1	62.08	0.70	7.99	2.57	51.24	69.62
BL7_T2	57.35	0.65	9.09	2.25	45.46	65.1
BL7_T3	62.86	0.67	4.10	3.40	56.47	67.14
BL8	64.97	0.77	6.94	2.58	49.73	76.66
BL9	74.90	0.81	3.69	5.02	67.93	80.51
BL10	70.36	0.75	3.64	4.53	64.05	75.10
BL10_T4	64.04	0.68	6.46	4.49	50.51	68.21
BL11	76.71	0.84	4.52	5.09	68.41	83.65

4.2.4. Energetics, grain size, and ejection velocities

Our experimental setups (1 and 2; Fig. 6) aimed to simulate two different scenarios (Section 3.2.3) in which the flashing of liquid water produced during decompression provides the energy for the unloading, eventual fragmentation, and ejection of loose material (Montanaro et al., 2016a, 2016b; Mayer et al., 2017). In both setups, the sample water content is the main parameter affecting the ejection dynamics of the particles (Mayer et al., 2015; Montanaro et al., 2016a, 2016b). In respect to the amount of water within the system observed, the associated explosive energy due to the work of the rapid expansion of the fluids (steam) can be estimated with respect to the experimental conditions, and by using a thermodynamic irreversible approach (details in the Supplementary Material; Thiéry and Mercury, 2009; Montanaro et al., 2016a, 2016b). For our experiments, the produced steam fraction varies between 2.05 and 4.01% for the 2.8/3.2 bars and 120 °C condition (Setup 1), and from 10.46 to 12.43% for the 9/16 bars and 150 °C condition (Setup 2). Thus, the estimated steam fractions served to determine the irreversible explosive energy (Eq. A.4 in Supplementary Material), reported in Table 2 as per unit volume of fluid ($E_{Unit\ vol.}$). For low pressure/temperature experiments, the 0.013–0.014 kg of water retained by the saturated loose material equates to an explosive energy of 1.5 to 3.5 MJ/m^3. Under higher pressure/temperature conditions, less saturated material with 0,0061–0.0087 g of water yielded explosive energies of 4.3 and 5.0 MJ/m^3. Samples retaining 0.0113–0.0171 g of water, instead, permitted an energy release of 7.7 to 10.2 MJ/m^3.

The grain-size distribution of the recovered material was analyzed and compared to that prior to the experiment. Grain-size distributions of the ejected samples from Setup 1 (BL1_11, BL1_12, BL5_5) exhibit a decreased weight fraction of ash-sized particles than the original sample (Figs. 10 and 11 and Suppl. mat. Figs. A.5 and A.6). Median diameters, compared to the initial grainsize, shift from 1 to 2 mm, respectively. For Setup 2 some samples also showed a decrease in ash fraction. Median diameters of BL6 and BL9_2 increase from 0.25 mm to 0.5 mm and the median of BL9_4 and BL10 rises from 0.25 to 0.355. On the contrary, an increase in amount of ash compared to initial sample grainsize is observed for BL7_1 and BL8 within Setup 2. In this case mean diameters of newly-produced material shift from 1.4 mm to

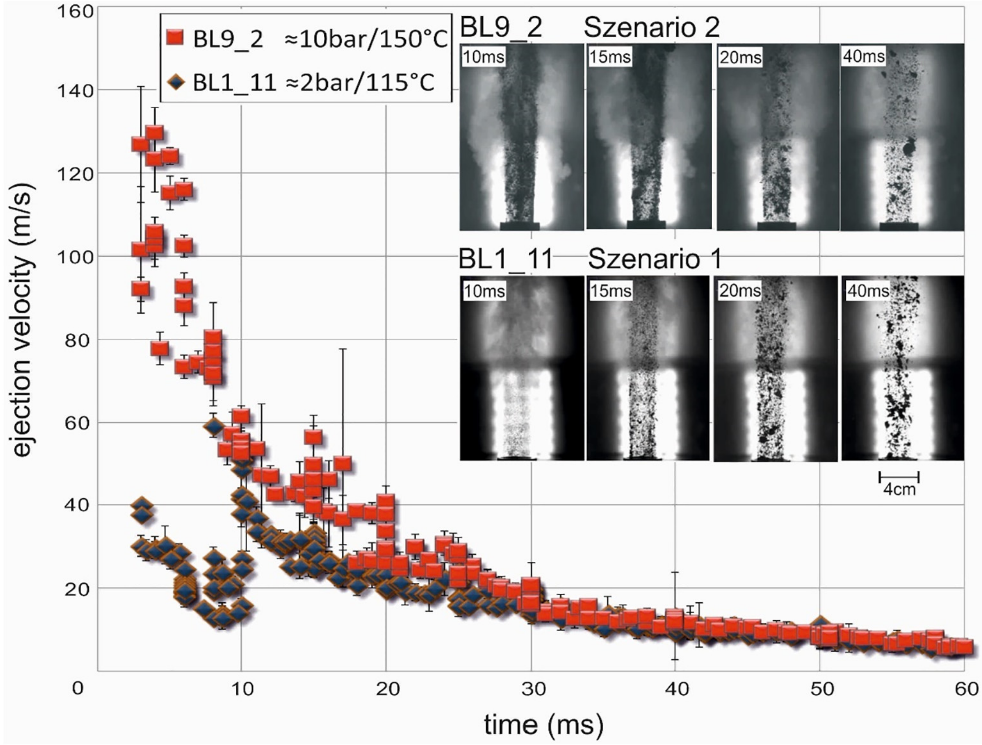

Fig. 9. Pictures of the time series from decompression experiments recorded with a high-speed camera combined with a diagram showing the ejection velocity of particles over time. Setup 1 (drainage event) is presented by BL1_11 and Setup 2 (landslide event) is shown by BL9_2. Particle ejection of BL9_2 starts earlier and the particle stream looks much denser and more energetic compared to BL1_11. Further differences are clearly visible in the diagram below. Ejection velocity of BL1_11 is much less and show an acceleration phase.

0.5 mm, respectively. Overall the particle size distribution is more uniformly graded after decompression experiments (Fig. 10, Suppl. mat. Fig. A.5 and A.6).

In the first setup the material ejected in the particle collection tank appeared turbid, with the presence of agglomerated material (Suppl. mat. Fig. A.7, type 5), not present in the initial mixture. These agglomerates consist of weakly-connected, very fragile and highly-breakable assemblages of finer grains. For Setup 1 loose material was filled into the sample holder and the ejected grains maintained a significant amount of moisture due to reduced vaporization at lower temperature conditions. Both factors favor the aggregation of ejected material, and in particular of ash-sized particles (Figs. 10 and 11). In Setup 2 however, the increase in ash fraction may be an indication of fragmentation as well as other size-reducing processes such as disintegration of aggregates (Montanaro et al., 2016b). In this case, the drier mixture would reduce the possibility of aggregation, and more energetic eruptions may increase the possibility of collision and breaking of particles.

The ejection velocity of the gas/water-particle mixture was obtained from high-speed video footage of each experiment. Both velocity decay with time and ejection speed of particle front were measured and the results are shown in Figs. 9 and 11, and listed in Table 2. In general, results indicate that in all of the experiments particles smaller than 1 mm are ejected first and reach the highest ejection speeds of 60–180 m/s, whereas larger particles (>2 mm) are ejected at a later stage and show a velocity range of 50–100 m/s. Moreover, depending on the pressure/temperature conditions the initial ejected particles show different velocities. In particular, particles from Setup 1 exhibited lower ejection speeds of the particle front (22–54 m/s) as compared to those ejected using Setup 2 (89–132 m/s).

4.2.5. Estimation of ballistic trajectories

We estimated the potential height and horizontal distance reached by lapilli-sized material based on the experimentally measured ejection velocity. Results are listed in Table 2 and Suppl. mat. Table A.2, as well as shown in Fig. 12. The estimated trajectories are used to assess the likelihood of lapilli-sized particles to reach visited areas around the lake, such as the alluvial fan (shore), the visitor platform or the top of the eastern crater wall (Fig. 2). For simulations of hydrothermal eruptions occurring during or after drainage events (Setup 1), maximum heights (ejection angle of 65°) and horizontal distances (ejection angle of 45°) varies from 12.6 to 20.7 m to 23.8–34.3 m, respectively. In the more energetic scenario of an eruption triggered by landslide (Setup 2), simulations show maximum heights (ejection angle of 65°) ranging from 34.1 to 57.3 m and horizontal distances (ejection angle of 45°) between 49.2 and 95.4 m.

5. Discussion

5.1. Hydrothermal activity and alteration effects on crater wall stability

The formation of the Boiling Lake, and the spatial distribution of hydrothermal features in the surrounding area is likely controlled by its structural setting (Traineau et al., 2015), as was also proposed by Schöpa et al. (2011) for the nearby Valley of Desolation. However, the intensity and style of hydrothermal activity, and in particular the occurrence of hydrothermal explosive events, seem to be influenced by alteration processes and drainage events which affects the lake.

The debris apron surrounding the Boiling Lake depression, likely due to denudation and mass wasting from the crater wall and deposition at its bottom, as well as the erosional channels cutting the crater at the lake-inlet and outlet, suggest that modification to the crater topography occurred after its formation (Fig. 2). However, it can be assumed that the main hydrothermal vent has remained at the same location during the period 1880–2016 (Mayer et al., 2017; Durand, 2017). Such persistence of emission location has also been well-documented at the nearby Valley of Desolation, where it results from the occurrence of deep-

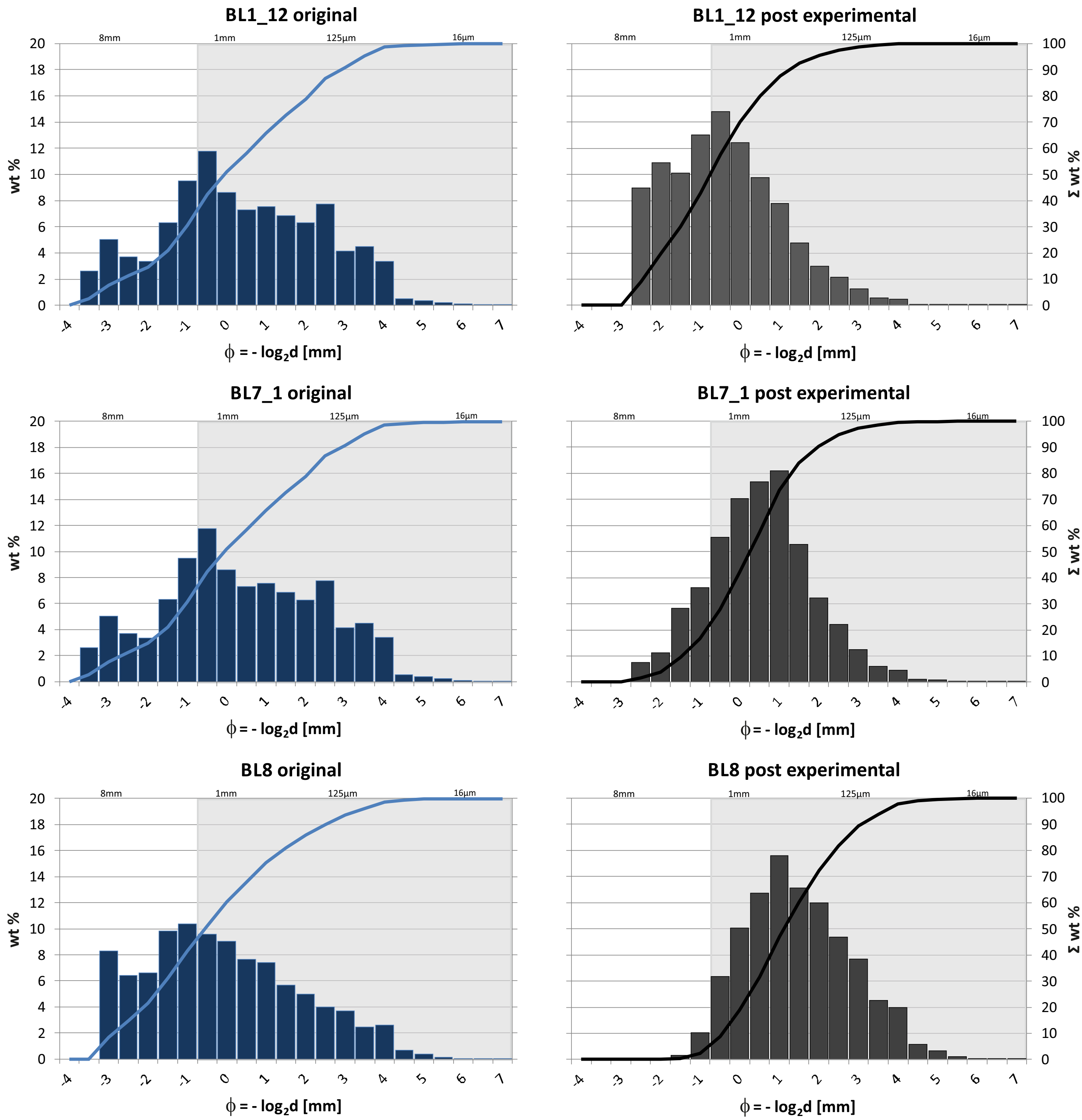

Fig. 10. GSD curves of original sample (blue) and post fragmented sample (grey). The shaded area highlights the ash fraction (particles below 2 mm). For BL1_12 (Setup 1) an agglomeration effect of finer particles is visible after decompression experiment. For BL7_1 and BL8 a higher amount of ash is generated during experiment. (For interpretation of the references to colour in this figure legend, the reader is referred to the web version of this article.)

seated, structurally controlled high-permeability pathways not affected by surficial modifications (Mayer et al., 2017; Harris and Maciejewski, 2000).

Together with weathering, intense hydrothermal/argillic alteration differently affects the crater walls thus favoring erosional and mass-wasting processes. Indeed, the alteration results in the formation of a clay-rich material, which exhibits a lower strength and is generally more easily eroded than consolidated rocks (Figueiredo et al., 1999).

Ongoing hydrothermal alteration has strong influences on rock mechanical and physical properties, as observed from the field and laboratory data collected in this study. The north crater wall, left of the alluvial fan (wall I) seems to be less altered than the walls to the right of the alluvial fan. The material composing the deposit show lowest values for alteration indices (e.g. CIA and CIW) and a low LOI, as well as an increased strength. It furthermore contains a higher amount of coarse grains (increased mode and median) compared to that of wall II and III. The deposit from the western wall III seems to be more affected by alteration. Samples BL8 and BL11, especially yield significantly low compaction/shear strength, which is in parallel with increased alteration indices. Except for BL8, all samples contain finer grains which

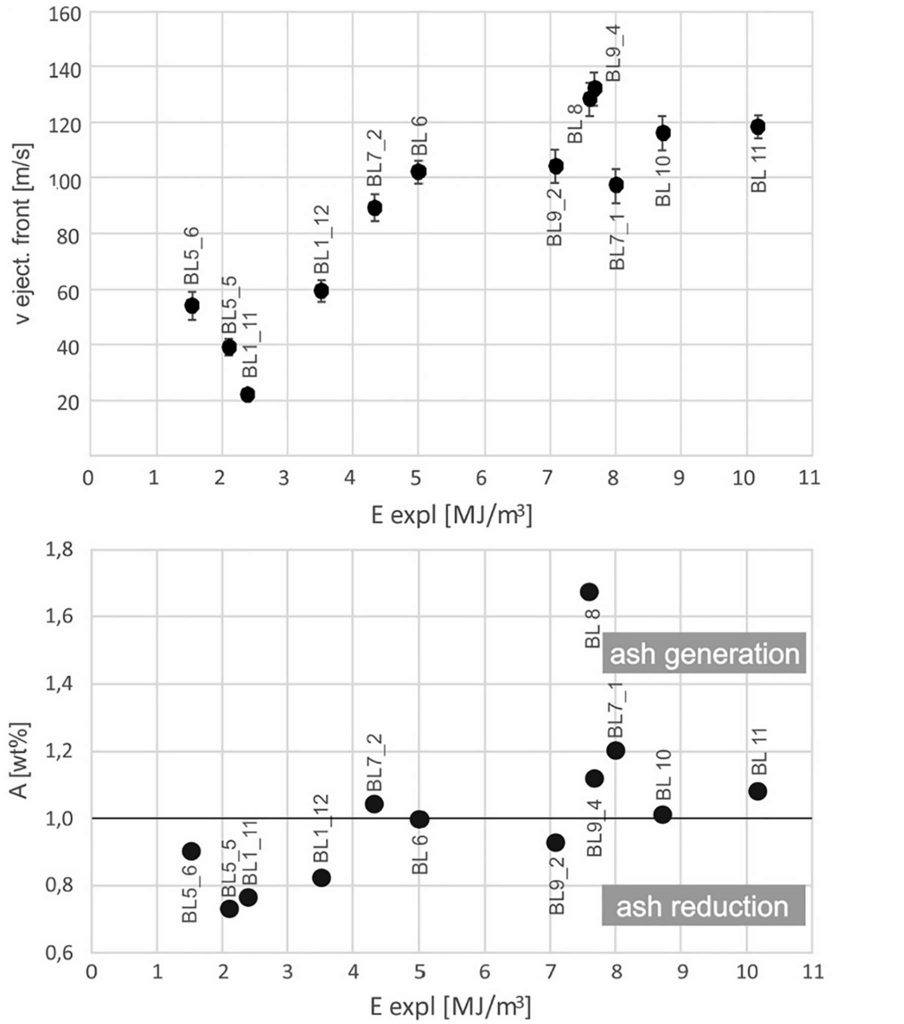

Fig. 11. The upper diagram shows the velocity of ejection front (fast particles at the beginning of ejection process) of as a function of irreversible explosive energy per volume. It is obvious that low energy samples, ejected with decreased pressure (BL1_11, BL1_12) or low water content (BL7_2) have lower velocities of ejection front compared to the other samples. Highest velocities are achieved by samples ejected at higher pressure ranges and which contain a large amount of water and a high porosity (BL11, BL8, BL10) or have a high alteration stage (BL11, BL9, BL10 CIA > 70). The lower diagram shows the generation or reduction of ash sized particles (<2 mm) referred to as *Ashiness Indicator* A (A = ash fraction after experiment divided by ash fraction prior experiment in wt%) also as a function of irreversible explosive energy per volume. Low pressure experiments (BL1_11 & BL1_12) as well as BL9_2 show agglomeration. Most of higher pressure experiments generates more ash particles in particular sample BL8 which material has the highest porosity and permeability and the second highest water content.

possibly result from disaggregation of highly altered and fragile components (Suppl. mat. Figs. A.5 and A.6). Larger amounts of pore water may enhance both hydrothermal and supergene alteration that in time can impair the stability of the steep crater walls (Mayer et al., 2016; Mayer et al., 2017). These changes in wall robustness can in turn affect erosion and/or facilitate mass wasting of the crater wall material.

The erosion of very fine grains produced by the ongoing hydrothermal alteration results in large amount of material being transported into the lake and re-sedimented at the bottom. This fine sediment likely settles down during the drainage periods when ebullition and water circulation stops. Indeed, during the low lake levels the outcropping bottom is covered by a thick blanket of mud-like sediments (Fig. 2d). Lake drainage and refilling periods can vary in time (<24 h to several weeks). The lake initially totally or partially fills with cold water before hydrothermal activity restarts. With the resumption of boiling and degassing, the activity increase before the lake reaches its normal water levels and activity. Protracted refilling of the lake might favor explosive events as within an extended period of a "non-active stage" the mud-plug has time to compact reducing its permeability. Consequently, when activity of the hydrothermal system restarts with warming up of the groundwater, the mud-plug can possibly act as a degassing barrier, which might cause over-pressurization in the hydrothermal system and its release in explosive failure (Browne and Lawless, 2001; Montanaro et al., 2016b).

Mass wasting of crater wall materials, also favored by alteration, can result in the generation of a landslide that may partially, or totally, fill up the crater and the vent area. If a large amount of material is involved, the landslide body may keep an internal structure and a low permeability similar to the pre-slide condition. Considering the fact that the Boiling Lake is surrounded by extremely steep (almost vertical) crater walls having a maximum height of about 45 m (from lake bottom to crater wall top), a landslide event creating an up to 10-m-thick landslide body is not unlikely. Despite the fact that such events have not yet occurred, future instabilities may be induced by progressive alteration which weakens the wall rocks, or by a combination of alteration effect and extreme weather conditions and seismic activity (e.g., landslides events from steep slopes affecting the nearby Valley of Desolation during periods of intense rainfall). At other crater lakes of similar size as or larger than the Boiling Lake, for e.g. at Kasu Tephra Cone in Papua New Guinea (Wagner et al., 2003), or at Askja in Iceland (Schöpa et al., 2018), alteration of steep walls is known to be one of the main factors favoring mass-wasting processes. Such a landslide body covering

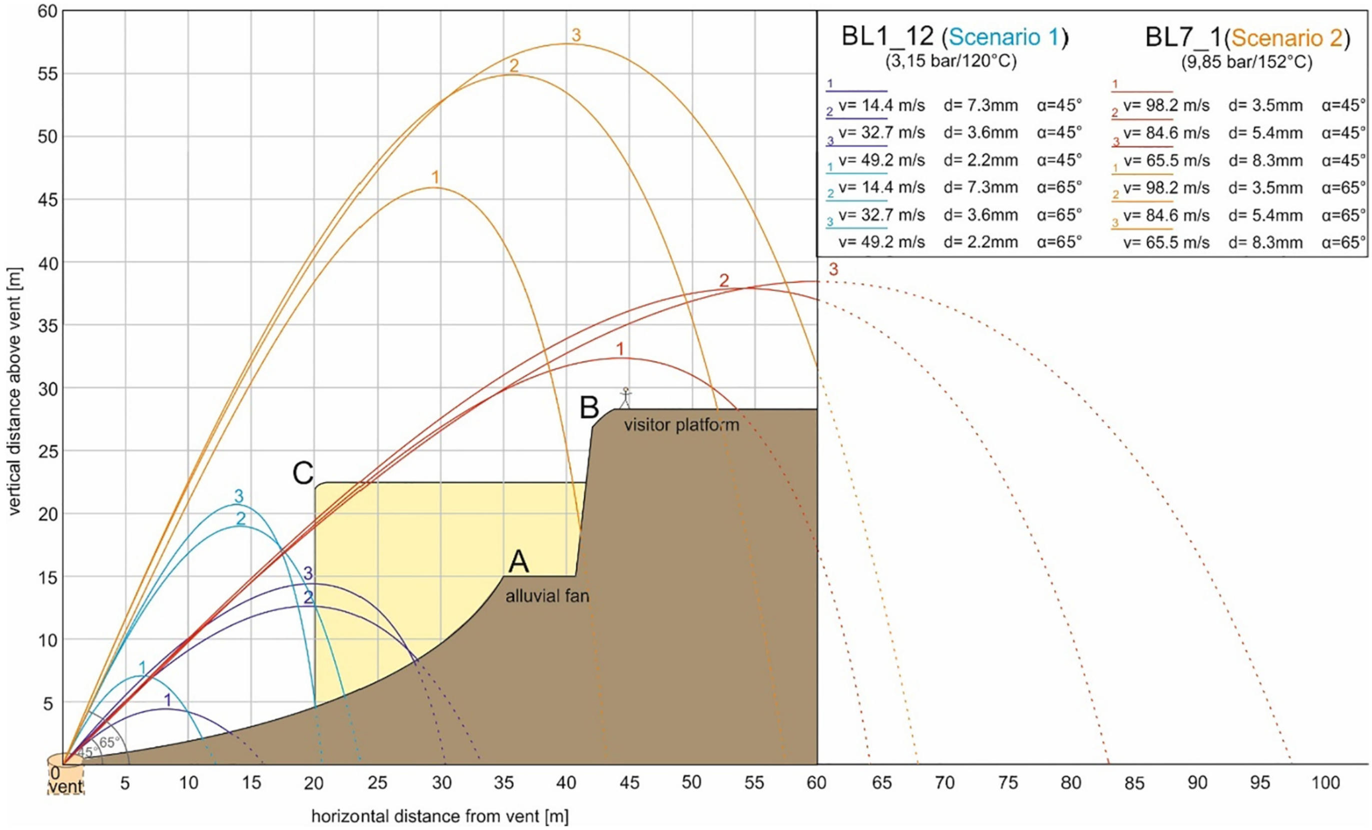

Fig. 12. The drawing illustrates ballistic trajectories of different sized fragments from two experiments driven under different P/T conditions. The figure shows the geometry of the Boiling Lake and the areas which would be affected by hydrothermal eruptions originating from the off-centered vent. Ballistics generated in BL1_12 (Scenario 1; decompression experiment with 3.15 bar & 120 °C) would not reach the shore A (alluvial fan) or the the visitor platform B but the crater wall C which was affected in Nov. 2016 by mud splatter. Ballistics ejected in decompression experiment with 9.85 bar and 152 °C (Scenario 2) reach area A, B and C and beyond. Point A, B and C are also marked in Fig. 3. Respectively three different sized particles with various velocities per experiment are used with an ejection angle of 45° and 65°.

the still active vent would lead to a pressure build up due to the rising hot fluids. After a period of time, and depending on the formation of fractures in the landslide body, the eruption may be driven by flashing of pressurized hot fluid, or by expanding over-pressurized gas overcoming the body yield strength (Browne and Lawless, 2001; Mayer et al., 2017).

Both the scenarios described above were used as likely-scenarios for the decompression experiments in this study (Section 3.2.3).

5.2. Explosion energetics and ejection dynamics of altered unconsolidated material

Hydrothermal eruptions involve the conversion of thermal energy stored in water into mechanical energy (Mastin, 1995; Browne and Lawless, 2001). The heated and pressurized water within factures and pores of the hosting lithology powers the fragmentation/unloading of the enclosing material and the ejection of debris. In this case, initial pressure/temperature as well as the amount of liquid fraction and connected porosity are the main parameters affecting i) the amount of stored explosive energy, and ii) the produced grain size and the kinetic energy imparted to the ejected material (Scheu et al., 2006; Thiéry and Mercury, 2009; Montanaro et al., 2016a, 2016b).

In the case of Boiling Lake we used loose or slightly consolidated ash and block flow material with a wide range of porosities (30–66%) and an average water content of 12 g. Such amount of water accounts for an explosive energy of 2.3 kJ/kg in case of plug explosion (Setup 1), and 7.0 kJ/kg in case of an eruption involving the original crater wall rocks (Setup 2). Comparable explosive energies have been estimated for small hydrothermal eruptions triggered by drainage at Gengissig Lake in Iceland (Montanaro et al., 2016b). At Gengissig the pressure failure led to the boiling of surficial fluids, while the presence of clay levels intercalated to coarse lake sediments favored the pressure build-up upon failure (Montanaro et al., 2016b). If a similar mechanism can be assumed for the drainage-driven eruptions at the Boiling Lake, we can envisage a failure of the mud cap, and the formation of a boiling-front penetrating downwards into the mud-filled conduit (Figs. 4 and 6), followed by the explosion front, where the steam expands, fragmenting/dragging and dispersing the surrounding material. In such a case, eruption continues until the rate of water boiling decreases and steam expansion ceases to provide sufficient energy to eject rocks from the crater (McKibbin et al., 2009; Montanaro et al., 2016b).

Ejection front velocities measured from drainage scenario case (Setup 1) are of ~ 60 m/s for ash-sized particles, and 25 m/s for lapilli (Table 2). These velocities are appreciably lower than for clasts ejected at Gengissig, where ash-sized particles reached 100 m/s and lapilli-sized one were ejected at 50 m/s, over a ballistic distance of 50–100 m. The difference in ejection velocities may be due to i) the slightly lower pressure/temperature conditions estimated for the Boiling Lake, and/or ii) the different lithologies involved in the eruption. Moreover, the lower pressure/temperature conditions used for Boiling Lake samples yield mixtures of higher water content which favor the aggregation of ejected material forming coarse ash-sized particles, and thus resulting in lower ejection velocities (Figs.11 and 12). Consequently, the distances for particles ejected from the Boiling Lake, estimated without accounting for wind speed, are shorter (max 35 m) but still comparable to those from the Gengissig eruption. For the mud spatter observed in November 2016, which resulted from a drainage-like scenario, only a few pictures are available showing the ejecta after this "explosive" event at the Boiling Lake suggesting that ash-to-lapilli sized fragments were likely ejected. If that remains true, the distance reached by such material would be in good agreement with our results. Unfortunately, the south-eastern crater wall was inaccessible during our last campaign and therefore sampling to confirm grain size at this wall was impossible.

For the landslide-triggered eruption, we used samples collected from the crater walls to represent the inner portion of a landslide body covering the vent area. Such samples show a wide range of lithology, porosity (30.9 to 66.3%) and water saturation (31.8 to 81.0%; m_{lab} in Table 1) combined with a relatively low permeability (~10^{-15} m^2). Water saturation in particular varies from 31.8 vol% (BL6) to 61.2 vol% (BL10) and 81 vol% (BL11), in agreement with the estimated sample porosity (from 30.9 to 56.9%). In terms of associated explosive energy, the more porous and saturated material is 2 to 2.5 times more explosive than the drier ones.

In terms of velocity, ejected particles reach different values that are dependent on porosity, water content and degree of alteration. At the Valley of Desolation, about 1 km southwest of the Boiling Lake, a hydrothermal eruption was also triggered by the burial of fumarolic vents by a 2.5–3 m thick landslide in 1997 (James 2013, personal communication, Mayer et al., 2017). The mass movement from this event, led to a pressurization of the hydrothermal system and resulted in a small volume hydrothermal eruption (James, 1997; Mayer et al., 2017). The eruption involved a few tons of erupted material and a new "Mini Valley" was formed (observations made by James, 1997). Decompression experiments were driven under P/T conditions of 3–5 bar and 115–125 °C. Fragmentation and/or unloading of such material resulted in the ejection velocities of 80 m/s for ash and 50 m/s for lapilli. Calculated trajectory distances of ejected particles are smaller for the "Mini Valley" eruption (max. 65 m) than for the landslide scenario applied for Boiling Lake experiments (up to 100 m). This is because we assumed a landslide body 10 m thick burying the vent. At Boiling Lake we can assume a landslide affecting the near vertical eastern side (where the 2016 small landslide occurred) and resulting in a 10 m thick body, at least ~30 m long (to be able to reach the vent) and ~20 m wide. Such a body, made of slightly consolidated rock material with high water content, will have a volume of ~6000 m^3 and produce overpressure conditions up to 10 bar. Therefore, experiments were done at an initial condition of approx. 10 bar and 150 °C. This condition leads to faster ejection velocities of particle front by an average of 140 m/s for ash and 100 m/s for lapilli thus resulting in a larger area affected by potential ejecta. We note here that agglomeration has been observed in our experiments. Accounting for it may affect the estimated ejection heights and distances. By increasing the ejected particle size through agglomeration, for. e.g. a change of grain size distribution mode from 1.4 to 2.6 mm, a reduction in velocity from 24 to 12 m/s is estimated, thus resulting in smaller heights (2.9 m instead of 5.7 m) and shorter distances (9.7 m instead of 13.9 m) being reached by the ejected particles. Moreover, the assumed clay-plug and the landslide body can be expected to be heterogeneous in terms of water-to-clay volume ratio. Such parameter may control the manner by which the wet body ruptures and thereby the velocity of the ejected particles, i.e. by producing more liquid-like droplets/agglomerates that are ejected slowly, or solid, angular fragments that are rapidly blasted out (Schmid et al., 2017). Qualitative observations on the high-speed videos confirm that, independent of experimental pressure/temperature conditions, a more liquid-like behavior can be observed for material >2 mm-sized, ejected later in the explosion (see for e.g. Fig. 9) and having ejection speed lower than 40 m/s. Therefore, heights and distances similar to those estimated for scenario 1 can be expected for liquid-rich agglomerated particles.

Other examples for the formation of overpressure by steam produced underneath a rock body are "rootless explosions/eruptions". These are also known as secondary eruptions and have happened, for example, after pyroclastic flows originating at Mount St. Helens in May 1980. Hot material of the debris avalanche flow covered ponds and small lakes. Steam was then generated by the contact of meteoric water with hot rocks. The pressure was built up for weeks and month before it overcame the strength and resistance of overlying rock material which finally exploded (Walker, 1983).

Results from the investigated scenarios in this work allow us to estimate the potential areas at risk of being impacted by debris ejection. In the event of an eruption associated with drainage events, it can be expected that very wet and hot material (e.g. mud slurry) is ejected over an area of about 3850 m^2, if assumed a circular distribution of the debris for a maximum horizontal distance of 35 m. In this event, neither the alluvial fan nor the visitor platform would be at risk of being impacted by the ejected material (Fig. 12). However, factors like the mud plug thickness, or the amount of non-condensable gas associated with the rising fluid may change the initial overpressure, and in turn the explosive energy (Mayer et al., 2015; Hurwitz et al., 2016). This may result in a larger area impacted by the ejected material. In terms of the landslide hazard scenario a considerably larger area of about 28,350 m^2 would be affected by debris projectiles assuming a horizontal impact distance up to 95 m (Table 2). The Boiling Lake itself, as well as the surrounding area, would be largely destroyed or transformed in such a case. A hydrothermal eruption at the Boiling Lake would not endanger villages, towns or infrastructure except for its hiking trail. It must be kept in mind, that the moisture of sample material, which is involved in scenario 2, is thought to be similar to experimental conditions used for rocks in this study. This study investigates only two possible trigger mechanisms for eruptions at Boiling Lake. However, there are only limited observations at the Boiling Lake, meaning that some explosive events might have occurred without external trigger, being originated from different causes. For instance, mineral sealing of the permeable conduit is not to be excluded, and would need no external triggers to result in an explosive failure (Browne and Lawless, 2001).

Experimental uncertainties may influence our results in the following manner. Due to likely water loss during the transport process, the measured water saturation in the laboratory is lower. Moreover, it should be considered that the landslide material might be saturated additionally with the lake water itself and in times of rainy seasons it would have in general a larger water content. Consequently, the full explosive potential could be underestimated and ejected debris can reach greater distances. An additional point is that for the drainage-driven scenario loose wall rock is used instead of original lake bed material which would probably show a different ejection behavior. This would be a desirable material to analyze; however the crater lake bed could only be sampled in periods of drainage and thus was not accessible within this study. We also ignore in this study the possibility of a directed blast e.g. caused by a partly clogged vent which would end up in a more energetic eruption towards a particular direction.

The presence of large clasts, e.g. in block size, have not been considered in the experiments and simulations performed for this study. However, impacts from block projectiles are amongst the most frequent causes of fatal volcanic incidents in general (Blong, 1984; Fitzgerald et al., 2017). Therefore, our estimation should be considered as the minimum area of impact in case of eruptions at Boiling Lake. Finally, it cannot be excluded that hydrothermal eruption dynamics evolve with time into much more energetic phreatomagmatic eruptions as it happened at Ruapehu, New Zealand (Christenson, 2000). This transition would affect a much larger area and involve greater risks.

6. Summary and conclusion

We explore trigger mechanisms and dynamics of hydrothermal eruptions at unstable crater lakes exemplified at, but not limited to the Boiling Lake in Dominica. The Boiling Lake displays an irregular occurrence of drainage events, sometimes followed by hydrothermal eruptions. Field analysis like in-situ permeability measurements and strength tests combined with laboratory experiments were carried out in order to characterize the crater wall material and to investigate the ejection behavior of particles, as well as the area affected in an explosive event. Results of transmitted light microscopy and componentry reveal the predominantly high alteration stage of crater wall material. In analogy to Mayer et al. (2016) we consider that alteration of rock due to hydrothermal activity and weathering could lead to increased formation of fine-grained material and strength reduction, thus favoring erosional and mass-wasting processes. Wall-eroded clays may plug the vent during drainages leading to overpressurized conditions, while mass-wasting from the altered crater walls may result in landslides clogging the degassing vent.

Rapid decompression experiments simulate the ejection dynamics I) in case of a small hydrothermal eruption initiated by a lake drainage event (Setup 1) as well as II) hydrothermal eruptions induced by landslides (Setup 2) (Fig. 6). Ejection velocity increases with increasing decompression pressure, porosity, degree of alteration and sample water content. Ballistic modeling calculations provide information about the range that ejected particles could reach and based on these results a hazard zone around the lake can be proposed. Field observations suggest that large amounts of fine material are produced by hydrothermal alteration which is easily eroded and transported into the lake. The large amount of mud thus produced likely deposits at the lake bottom during drainages favoring the "mud plug mechanism" trigger for creating overpressurized conditions and, in turn, explosions. However, experimental velocities and vent position used for modeling suggest that the overpressured system may explode ejecting lapilli-sized material up to 30–35 m distance, thus not likely to impact on the visitor platform located almost 42 m NW of the vent. The 2016 event ejected debris on the eastern wall which is only about 20 m away from the visitor platform. If a thicker mud plug is formed, or higher pressures and temperatures are reached before the failure, it can be expected that larger distances may be reached by the ejected clasts thus impacting on the visitor platform or the alluvial fan (shore). Alternatively, ejected particles of an event with higher pressure/temperature conditions, like a hydrothermal eruption induced by a landslide body of about 10 m thickness, are able to reach the visitor platform as well as the surrounding area (Fig. 12). The emission of toxic gases, particularly CO_2, during eruption events and the formation of very fine ash particles presents a further danger to human life.

Phreatic or hydrothermal eruption in active hydrothermal fields in Dominica as the area around the Valley of Desolation and the Boiling Lake have a frequency about once per century. For this reason, a phreatic or hydrothermal eruption may occur in the next 30 years and is almost certain within 100 years (Lindsay et al., 2005a). There are several worthy avenues for future research: (1) Incorporate chemistry into the decompression experiments by allowing for mixed phases and/or brines, and (2) To expand the study of the shallow hydrothermal system below the Boiling Lake and neighboring hydrothermal active areas (e.g. Traineau et al., 2015). For example Electrical Resistivity Tomography could shed more light on hydrothermal structures beneath the lake and their mechanism of behavior as shown in the study of Gresse et al. (2017) on Solfatara crater (Italy). Additionally, enhanced geochemical monitoring, further characterization of hydrothermally affected materials and additional decompression experiments under varying pressure and temperature conditions as well as with different kinds of crater rocks would be useful for the area around the Boiling Lake but also for other regions characterized by active volcano-hydrothermal systems.

Acknowledgements

This project has received funding from the European Union Seventh Framework Programme for research, technological development, and demonstration under grant agreement no. 282759 (VUELCO). We thank S. Müller for assistance during the field work and D. Aßbichler for XRF analysis. We acknowledge J. Arlington for personal reports on activity in the study area and the helpful photographic material (Fig. 2c). The authors wish to thank the Division of Forestry, Wildlife and National Parks of Dominica for the sampling permission. This manuscript has benefitted from constructive reviews by J. Vandemeulebrouck, J. Stix and N. Fournier.

Appendix A. Supplementary data

Supplementary data to this article can be found online at https://doi.org/10.1016/j.jvolgeores.2019.05.020.

References

Alatorre-Ibargüengoitia, M.A., Scheu, B., Dingwell, D.B., Delgado-Granados, H., Taddeucci, J., 2010. Energy consumption by magmatic fragmentation and pyroclast ejection during Vulcanian eruptions. Earth Planet. Sci. Lett. 291 (1–4), 60–69.

Alidibirov, M., Dingwell, D.B., 1996. An experimental facility for the investigation of magma fragmentation by rapid decompression. Bull. Volcanol. 58 (5), 411–416.

Arikan, F., Ulusay, R., Aydın, N., 2007. Characterization of weathered acidic volcanic rocks and a weathering classification based on a rating system. Bull. Eng. Geol. Environ. 66 (4), 415–430.

Blong, R.J., 1984. Volcanic Hazards: A Sourcebook on the Effects of Eruptions. Academic Press, Orlando.

Browne, P.R.L., Lawless, J.V., 2001. Characteristics of hydrothermal eruptions, with examples from New Zealand and0 elsewhere. Earth Sci. Rev. 52, 299–331.

Caudron, C., Taisne, B., Neuberg, J., Jolly, A.D., Christenson, B., Lecocq, T., Suparjan, Syahbana, D., and Suantika, G., 2018, Anatomy of phreatic eruptions: Earth Planets Space, v. 70, p. 168, doi:https://doi.org/10.1186/s40623-018-0938-x.

Christenson, B.W., 2000. Geochemistry of fluids associated with the 1995–1996 eruption of Mt. Ruapehu, New Zealand: signatures and processes in the magmatic–hydrothermal system. J. Volcanol. Geotherm. Res. 97, 1–30.

Criaud, A., Fouillac, C., 1989. The distribution of arsenic (iii) and arsenic (v)in geothermal waters: examples from the massif central of France, the island of Dominica in the leeward islands of the Caribbean, the valles caldera of new Mexico, U.S.A., and southwest Bulgaria. Chem. Geol. 76, 259–269, 1989.

DeMets, C., Jansma, P.E., Mattioli, G.S., Dixon, T.H., Farina, F., Bilham, R., Calais, E., E., Mann, P., 2000. Gps geodetic constraints on Caribbean-north America plate motion. Geophys. Res. Lett. 27 (2000), 437–440.

Di Napoli, R., Aiuppa, A., Allard, P., 2013. First multi-gas based characterization of the Boiling Lake volcanic gas (Dominica, Lesser Antilles). Ann. Geophys. 56 (5), S0559.

Dixon, T.H., Farina, F., DeMets, C., Jansma, P., Mann, P., Calais, E., 1998. Relative motion between the Caribbean and north American plates and related boundary zone deformation from a decade of gps observations. J. Geophys. Res. 103 (1998), 15157–15183.

Durand, S., 2016. Notes on Field Trip to Boiling Lake: 11th November, 2016. Forestry, Wildlife & Parks Division, Roseau, Dominica.

Durand, S., 2017. Report on Monitoring of the Valley of Desolation and the Boiling Lake: 26th January, 2017. Forestry, Wildlife & Parks Division, Roseau, Dominica.

Duzgoren-Aydin, N.S., Aydin, A., Malpas, J., 2002. Re-assessment of chemical ewathering indices: case study on pyroclastic of Hong Kong. Eng. Geol. 63, 99–119.

Farquhar, G., 2001. Guideline for Held Shear Vane Test. New Zealand geotechnical Society.

Feuillet, N., Beauducel, F., Jacques, E., Tapponnier, P., Delouis, B., Bazin, S., Vallée, M., King, G.C.P., 2011. The Mw = 6.3, November 21, 2004, Les Saintes earthquake (Guadeloupe): tectonic setting, slip model and static stress changes. J. Geophys. Res. 116 (B10), 1–25.

Figueiredo, M.A., Augustin, C., Fabris, J.D., 1999. Mineralogy, size, morphology and porosity of aggregates and their relationship with soil susceptibility to water erosion. Hyperfine Interact. 122, 177–184.

Fitzgerald, R.H., Kennedy, B.M., Wilson, T.M., Leonard, G.S., Tsunematsu, K., Keys, H., 2017. The communication and risk management of volcanic ballistic hazards. Advances in Volcanology. Springer Berlin Heidelberg, Berlin, Heidelberg, pp. 1–27 https://doi.org/10.1007/11157_2016_35.

Fournier, N., Witham, F., Moreau-Fournier, M., Bardou, L., 2009. Boiling Lake of Dominica, West Indies: High temperature volcanic crater lake dynamics. J. Geophys. Res. Solid Earth 114 (B2).

González, G., Mora-Amador, R.A., Ramírez, C.J., Rouwet, D., 2013. Variations in physicchemical features and seismicity related to phreatic activity for the two active crater lakes in Costa Rica: Poás and Rincón de la Vieja volcanoes. 8thWorkshop on Volcanic Lakes. IAVCEI Commission on Volcanic Lakes, Japan, p. 36.

Gresse, M., Vandemeulebrouk, J., Byrdina, S., Chiodini, G., Revil, A., Johnson, T.C., Ricci, T., Vilardo, G., Mangiacapra, A., Lebourg, T., Grangeon, J., Bascou, P., Metral, L., 2017. 3-D electrical resistivity tomography of the Solfatara crater (Italy): implication for the multiphase flow structure of the shallow hydrothermal system. J. Geophys. Res. Solid Earth, 122 https://doi.org/10.1002/2017JB014389.

Harris, A.J.L., Maciejewski, A.J.H., 2000. Thermal surveys of the Vulcano Fossa fumarole field 1994-1999: evidence for fumarole migration and sealing. J. Volcanol. Geotherm. Res. 102 (1–2), 119–147.

Heap, M.J., Kennedy, B.M., Farquharson, J.I., Ashworth, J., Mayer, K., Letham-Brake, M., Reuschlé, T., Gilg, H.A., Scheu, B., Lavalée, Y., Siratovich, P., Cole, J., Jolly, A.D., Baud, P., Dingwell, D.B., 2017. A multidisciplinary approach to quantify the permeability of the Whakaari/White Island volcanic hydrothermal system (Taupo Volcanic Zone, New Zealand). J. Volcanol. Geotherm. Res. 332, 88–108.

Hurst, T., Jolly, A.D., Sherburn, S., 2014. Precursory characteristics of the seismicity before the 6 August 2012 eruption of Tongariro volcano, North Island, New Zealand. J. Volcanol. Geotherm. Res. 286, 294–302.

Hurwitz, S., Clor, L.E., McCleskey, R.B., Nordstrom, D.K., Hunt, A.G., Evans, W.C., 2016. Dissolved gases in hydrothermal (phreatic) and geyser eruptions at Yellowstone National Park, USA. Geology 44. https://doi.org/10.1130/G37478.1 G37478.1.

James, A., 2014. What was said in Dominica's Newspapers about the Boiling Lake's 1988 and 2004/05. episodes. "Cool-Down".

James, A., 1997. Observations Made in the Valley of Desolation Following a Volcanic Eruption, July 1997. (Unpublished report). Forestry and Wildlife Division, Dominica.

James, A., 2005. Reports Made from Monitoring of the Boiling Lake 28th December 2004 to 13th April 2005.

Joseph, E.P., Fournier, N., Lindsay, J.M., Fischer, T.P., 2011. Gas and water geochemistry of geothermal systems in Dominica, Lesser Antilles island arc. J. Volcanol. Geotherm. Res. 206 (1), 1–14.

Joseph, E.P., Frey, H.M., Manon, M., Onyeali, M.-M., DeFranco, K., Metzger, T., Aragosa, C., 2019. Update on the fluid geochemistry monitoring time series for geothermal systems in Dominica, Lesser Antilles. J. Volcanol. Geotherm. Res. 36, 86–103. https://doi.org/10.1016/j.jvolgeores.2019.03.010.

Kilgour, G., Manville, V., Della Pasqua, F., Graettinger, A., Hodgson, K.A., Jolly, G.E., 2010. The 25 September 2007 eruption of Mount Ruapehu, New Zealand: directed ballistics, surtseyan jets, and ice-slurry lahars. J. Volcanol. Geotherm. Res. 191, 1–14.

Kiryukhin, A., Rychkova, T., Dubrovskaya, I., 2012. Formation of the hydrothermal system in Geysers Valley (Kronotsky Nature Reserve, Kamchatka) and triggers of the Giant Landslide. Appl. Geochem. 27 (9), 1753–1766.

Lindsay, J.M., Stasiuk, M.V., Shepherd, J.B., 2003. Geological history and potential hazards of the late-Pleistocene to recent Plat Pays volcanic complex, Dominica, Lesser Antilles. Bull. Volcanol. 65 (2–3), 201–220.

Lindsay, J.M., Smith, A.L., Roobol, M.J., Stasiuk, M.V., 2005a. Dominica. In: Lindsay, J.M., Robertson, R.E.A., Shepherd, J.B., Ali, S. (Eds.), Volcanic Hazard Atlas of the Lesser Antilles-Seismic Research Unit. The University of the West Indies, Trinidad and Tobago, W.I, pp. 1–48.

Lindsay, J.M., Trumbull, R.B., Siebel, W., 2005b. Geochemistry and petrogenesis of late Pleistocene to recent volcanism in South Dominica, Lesser Antilles. J. Volcanol. Geotherm. Res. 148, 253–294.

Lowenstern, J.B., van Hinsberg, V., Berlo, K., Liesegang, M., Iacovino, K., Bindeman, I.N., Wright, H.M., 2018. Opal-A in glassy pumice, acid alteration, and the 1817 phreatomagmatic eruption at KawahIjen (Java), Indonesia. Front. Earth Sci. 6, 11. https://doi.org/10.3389/feart.2018.00011.

Mastin, L.G., 1995. Thermodynamics of gas and steam-blast eruptions. Bull. Volcanol. 57 (2), 85–98.

Mastin, L.G., 2001. A simple calculator of ballistic trajectories for blocks ejected during volcanic eruptions. U.S. Geol. Surv. Open File Rep. 01–45 (16p).

Maury, R.C., Westbrook, G. K., Baker, P.E., Bouysse P., Westercamp D.,(1990). The Lesser Antilles. G. Dengo and J. Case (eds.), Decade of North American Geology, H, The Caribbean Region, Geological Society America, pages 141–166, vol. 1990.

Mayer, K., Scheu, B., Gilg, H.A., Heap, M.J., Kennedy, B.M., Lavallée, Y., Letham-Brake, M., Dingwell, D.B., 2015. Experimental constraints on phreatic eruption processes at Whakaari (White Island volcano). J. Volcanol. Geotherm. Res. 302, 150–162.

Mayer, K., Scheu, B., Montanaro, C., Yilmaz, T.I., Isaia, R., Aßbichler, D., Dingwell, D.B., 2016. Hydrothermal alteration of surficial rocks at Solfatara (Campi Flegrei): Petrophysical properties and implications for phreatic eruption processes. J. Volcanol. Geotherm. Res. 320, 128–143.

Mayer, K., Scheu, B., Yilmaz, T.I., Montanaro, C., Gilg, H.A., Rott, S., Joseph, E.P., Dingwell, D.B., 2017. Phreatic activity and hydrothermal alteration in the Valley of Desolation, Dominica, Lesser Antilles. Bull. Volcanol. 79, 82.

McKibbin, R., Smith, T.A., Fullard, L., 2009. Components and phases: modelling progressive hydrothermal eruptions. ANZIAM J. 50, 365–380.

Montanaro, C., Scheu, B., Mayer, K., Orsi, G., Moretti, R., Isala, R., Dingwell, D.B., 2016a. Experimental investigations on the explosivity of steam-driven eruptions: a case study of Solfatara volcano (Campi Flegrei). J. Geophys. Res. Solid Earth 121.

Montanaro, C., Scheu, B., Gudmundsson, M.T., Vogfjörd, K., Reynolds, H.I., Dürig, T., Strehlow, K., Rott, S., Reuschlé, T., Dingwell, D.B., 2016b. Multidisciplinary constraints of hydrothermal explosions based on the 2013 Gengissig lake events, Kverkfjöll volcano, Iceland. Earth Planet. Sci. Lett. 434, 308–319.

Montanaro, C., Mayer, K., Isaia, R., Gresse, M., Scheu, B., Yilmaz, T.I., Vandemeulebrouck, J., Ricci, T., Dingwell, D.B., 2017. Hydrothermal activity and subsoil complexity: implication for degassing processes at Solfatara crater, Campi Flegrei caldera. Bull. Volcanol. 79, 83.

Ober, F.A., 1880. Camps in the Caribbees: The Adventures of a Naturalist in the Lesser Antilles. Lee and Shepherd, Boston, US (Edinburgh: Douglas. (Reviewed in Nature July 8 1880 p215).

Pola, A., Crosta, G., Fusi, N., Barberini, V., Norini, G., 2012. Influence of alteration on physical properties of volcanic rocks. Tectonophysics 566, 67–86.

Pola, A., Crosta, G., Fusi, N., Castellanza, R., 2014. General characterization of the mechanical behaviour of different volcanic rocks with respect to alteration. Eng. Geol. 169, 1–13.

Rager, A.H., Smith, E.I., Scheu, B., Dingwell, D.B., 2014. The effects of water vaporization on rock fragmentation during rapid decompression: Implications for the formation on fluidized ejecta on Mars. Earth Planet. Sci. Lett. 385, 68–78.

Rouwet, D., Morrissey, M.M., 2015. Mechanisms of Crater Lake Breaching Eruptions. In: Rouwet, D., Christenson, B., Tassi, F., Vandemeulebrouck, J. (Eds.), Volcanic Lakes. Advances in Volcanology. Springer, Berlin, Heidelberg.

Rouwet, D., Mora-Amador, R., Ramírez-Umaña, C., 2010. A combined Cl and isotope balance approach for Laguna Caliente, Poás: Precursory signals for single phreatic eruptions during the ongoing eruptive cycle? 7th Workshop on Volcanic Lakes. IAVCEI Commission on Volcanic Lakes, Costa Rica (23)

Scheu, B., Spieler, O., Dingwell, D.B., 2006. Dynamics of explosive volcanism at Unzen volcano: an experimental contribution. Bull. Volcanol. 69 (2), 175–187.

Schmid, D., Sheu, B., Wadsworth, F.B., Kennedy, B.M., Jolly, A, Dingwell, D.B., 2011. A viscous-to-brittle transition in eruptions through clay suspensions. Geophys. Res. Lett. 44. https://doi.org/10.1002/2017GL073641.

Schöpa, A., Pantaleo, M., Walter, T.R., 2011. Scale-dependent location of hydrothermal vents: stress field models and infrared field observations on the Fossa Cone, Vulcano Island, Italy. J. Volcanol. Geotherm. Res. 203, 133–145.

Schöpa, A., Chao, W., Lipovsky, B.P., Hovius, N., White, R.S., Green, R.G., Turowski, J.M., 2018. Dynamics of the Askja caldera July 2014 landslide, Iceland, from seismic signal analysis: precursor, motion and aftermath. Earth Surf. Dyn. 6, 467–485.

Smith, A.L., Roobal, M.J., 2004. Geological Map of Dominica, West Indies. Geology Department, University of Puerto Rico, at Mayaquez.

Strehlow, K., Sandri, L., Gottsmann, J.H., Kilgour, G., Rust, A.C., Tonini, R., 2017. Phreatic eruptions at crater lakes: occurrence statistics and probabilistic hazard forecast. J. Appl. Volcanol., 21 https://doi.org/10.1186/s13617-016-0053-2.

Thiéry, R., Mercury, L., 2009. Explosive properties of water in volcanic and hydrothermal systems. J. Geophys. Res. 114, B05205.

Traineau, H., Lasne, E., Coppo, N., Baltassat, J.-M., 2015. Recent geological, geochemical and geophysical surveys of the Roseau Valley, high-temperature geothermal field in Dominica, West Indies. World Geothermal Congress 2015, Melbourne, Australia, p. 11.

Vandemeulebrouck, J., Stemmelen, D., Hurst, T., Grangeon, J., 2005. Analogue modeling of instabilities in crater lake hydrothermal systems. J. Geophys. Res. Solid Earth 110 (B2).

Vandemeulebrouck, J., Hurst, A., Scott, B., 2008. The effects of hydrothermal eruptions and a tectonic earthquake on a cycling crater lake (Inferno Crater Lake, Waimangu, New Zealand). J. Volcanol. Geotherm. Res. 178 (2), 271–275.

Wadge, G., 1984. Comparison of volcanic production rates and subduction rates in the Lesser Antilles and central America. Geology 12, 555–558.

Wadsworth, F.B., Unwin, H.E., Vasseur, J., Kennedy, B.M., Holzmueller, J., Scheu, B., Witcher, T., Adolf, J., Cáceres, F., Casas, A.S., Cigala, V., Clement, A., Colombier, M., Cronin, S., Cronin, M., Dingwell, B.D., Guimaraes, L.F., Höltgen, L., Kueppers, U., Seropian, G., Stern, S., Teissier, Vossen, C., Weichselgartner, N., 2018. Trashcano: developing a quantitative teaching tool to understand ballistics accelerated by explosive volcanic eruptions. Volcanica 1 (2), 107–126. https://doi.org/10.30909/vol.01.02.107126.

Wagner, T.P., McKee, C.O., Kuduon, J., Kombua, R., 2003. Landslide-induced wave in a small volcanic lake: Kasu Tephra Cone. Papua New Guinea. Int. J. Earth Sci. 92, 405–406.

Walker, G.P.L., 1983. Ignimbrite types and ignimbrite problems. In: Sheridan, M.F., Barberi, F. (Eds.), Explosive Volcanism. J. Volcanol. Geotherm. Res vol. 17, pp. 65–88.

Zimbone, S.M., Vickers, A., Morgan, R.P.C., Vella, P., 1996. Field investigations of different techniques for measuring surface soil shear strength. Soil Technol. 9 (1), 101–111.

Further reading

James, A., 2005. Reports Made from Monitoring of the Boiling Lake 28th December 2004 to 13th April 2005.

Umwelt-Geräte-Technik, 2012. PL-300 User's Manual. Version18.03.2014 (Müncheberg).

View publication stats